Journal of Sedimentary Research

# Provenance of modern sands from Baja California Rivers (Mexico): Petrographic constraints from light and heavy minerals

--Manuscript Draft--

| | |
|---|---|
| Manuscript Number: | 2022.052R5 |
| Article Type: | Research Article |
| Corresponding Author: | Anna Chiara Tangari<br><br>ITALY |
| First Author: | Emilia Le Pera, Associate Professor |
| Order of Authors: | Emilia Le Pera, Associate Professor |
| | Anna Chiara Tangari, Post Doctoral Researcher |
| | Lucia Marinangeli, Associate Professor |
| | Consuele Morrone, Post Doctoral Researcher |
| | Lars Riber, Researcher |
| | Sergio Andò, Associate professor |
| Abstract: | We used high-resolution petrographic and dense-mineral data on modern sand to investigate erosion patterns of El Rosario, San Fernando, and San Vicente rivers basins of the Baja California (Mexico) for better understanding the interrelationships between a complex magmatic arc terrane and surface processes. Modern sand composition of these three rivers reflects the nature of the source region, which lies in the central part of the Alisitos arc (Peninsular Ranges, Baja California, Mexico). The sand detrital modes correspond well with the main structural units drained by El Rosario, San Fernando, and San Vicente rivers: (1) the Early Cretaceous oceanic arc of the Alisitos Group, (2) the Paleozoic to Mesozoic continental margin metasedimentary rocks, (3) the Cretaceous plutons, (4) the Upper Cretaceous to Tertiary sedimentary rocks, and (5) the Tertiary volcanics. San Vicente, San Fernando, and El Rosario rivers modern sand is chiefly fed from erosion of a magmatic arc and mostly consists of minor feldspatho-lithic (Fl) to quartzo-litho-feldspathic (qFL) sand and dominant quartzo-feldspatho-lithic (qLF) and litho-feldspatho-quartzose (lQF) sand. Framework petrography also suggests a progressive increase in quartz, K-feldspar, sedimentary, and metamorphic lithic fragments, and decreasing in volcanic lithic fragments. Sand, within the Lv field, microlitic (Lvmi), contains felsitic (Lvf), and lathwork (Lvl) types, and trace amounts of vitric grains (Lvv), such as pumice particles. Andesitic volcanic province of the Alisitos arc shed quartz-poor sand containing mainly microlitic lithic fragments and plagioclase, whereas sand derived from more felsic rhyolites and rhyodacitic and trachyandesitic products contains largely felsitic volcanic lithics and minor lathwork lithics are mainly derived from subordinate basalts. The abundance of intrusive rock fragments and volcanic and sedimentary lithics of the sampled river sands faithfully represents the relative abundance of a heterogeneous bedrock exposure consisting of sedimentary/metasedimentary rocks, as well as volcanic, plutonic, and medium to high grade metamorphic rocks in each drainage basin. Transparent heavy-mineral assemblages including major amounts of amphibole, pyroxene, epidote, titanite, zircon, and minor amounts of staurolite, rutile, actinolite, tourmaline, garnet, kyanite, andalusite, sillimanite, and apatite are in good agreement with a mixed provenance characterized mainly by magmatic, primarily volcanic (andesite, rhyolite, and basalt) and secondarily plutonic (granitoid rocks) and metamorphic source rocks. Some labile species such as hornblende and pyroxene grains show mainly corroded to etched morphologies due to dissolution processes and by chemical weathering processes occurring in a paleo and current semi-arid climate. Zircon+Tourmaline+Rutile index of the heavy-mineral modes, coupled with their sub-rounded to rounded grain surface texture, indicates recycling from the sedimentary source rocks. Heavy-mineral abundance and weathering textures in San Fernando and San Vincente rivers sands match predominantly volcanic bedrock lithologies while El Rosario river sands match sedimentary and metasedimentary source rocks. |

# Provenance of modern sands from Baja California Rivers (Mexico): Petrographic constraints from light and heavy minerals

Le Pera Emilia[1], Tangari Anna Chiara[2*], Marinangeli Lucia[2], Morrone Consuele[1], Riber Lars[3] and Andò Sergio[4].

[1]*Dipartimento di Biologia, Ecologia e Scienze della Terra (DiBEST), Università della Calabria, Via P. Bucci, Cubo 15B, 87036 Arcavacata di Rende (CS), Italy*

[2]*Dipartimento di Scienze Psicologiche, della Salute e del Territorio (DiSPuTer), Università di Chieti-Pescara, 66100 Chieti, Italy*

[3]*Department of Geosciences, University of Oslo, P.O. Box 1047, Blindern, NO-0316 Oslo, Norway*

[4]*Dipartimento di Scienze dell'Ambiente e della Terra (DISAT), Università di Milano-Bicocca, Piazza della Scienza 4, 20126 Milano, Italy*

* Corresponding author: a.tangari@unich.it

## Abstract

We used high-resolution petrographic and dense-mineral data on modern sand to investigate erosion patterns of El Rosario, San Fernando, and San Vicente rivers basins of the Baja California (Mexico) for better understanding the interrelationships between a complex magmatic arc terrane and surface processes. Modern sand composition of these three rivers reflects the nature of the source region, which lies in the central part of the Alisitos arc (Peninsular Ranges, Baja California, Mexico). The sand detrital modes correspond well with the main structural units drained by the El Rosario, San Fernando, and San Vicente rivers: (1) the Early Cretaceous oceanic arc of the Alisitos Group, (2) the Paleozoic to Mesozoic continentalmargin metasedimentary rocks, (3) the Cretaceous plutons, (4) the Upper Cretaceous to Tertiary sedimentary rocks, and (5) the Tertiary volcanics. The modern sand of the San Vicente, San Fernando, and El Rosario rivers is fed chiefly from erosion of a magmatic arc

and consists mostly of minor feldspatho-lithic (Fl) to quartzo-litho-feldspathic (qFL) sand and dominant quartzo-feldspatho-lithic (qLF) and litho-feldspatho-quartzose (lQF) sand. Framework petrography also suggests a progressive increase in quartz, K-feldspar, sedimentary, and metamorphic lithic fragments, and decreasing in volcanic lithic fragments. Sand, within the Lv field, microlitic (Lvmi), contains felsitic (Lvf) and lathwork (Lvl) types, and trace amounts of vitric grains (Lvv), such as pumice particles. The andesitic volcanic province of the Alisitos arc shed quartz-poor sand containing mainly microlitic lithic fragments and plagioclase, whereas sand derived from more felsic rhyolites and rhyodacitic and trachyandesitic products contains largely felsitic volcanic lithics, and minor lathwork lithics are mainly derived from subordinate basalts. The abundance of intrusive rock fragments and volcanic and sedimentary lithics of the sampled river sands faithfully represents the relative abundance of a heterogeneous bedrock exposure consisting of sedimentary and metasedimentary rocks, as well as volcanic, plutonic, and medium-to high-grade metamorphic rocks in each drainage basin. Transparent heavy-mineral assemblages including major amounts of amphibole, pyroxene, epidote, titanite, zircon, and minor amounts of staurolite, rutile, actinolite, tourmaline, garnet, kyanite, andalusite, sillimanite, and apatite are in good agreement with a mixed provenance characterized mainly by magmatic, primarily volcanic (andesite, rhyolite, and basalt) and secondarily plutonic (granitoid rocks) and metamorphic source rocks. Some labile species such as hornblende and pyroxene grains show mainly corroded to etched morphologies due to dissolution processes and by chemical weathering processes occurring in a paleo and current semiarid climate. The Zircon+Tourmaline+Rutile index of the heavy-mineral modes, coupled with their subrounded to rounded grain surface texture, indicates recycling from the sedimentary source rocks. Heavy-mineral abundance and weathering textures in San Fernando and San Vincente rivers sands match predominantly volcanic bedrock lithologies, while El Rosario river sands match sedimentary and metasedimentary source rocks.

*Key words: volcaniclastic sand, magmatic arc, heavy minerals, volcanic provenance*

## INTRODUCTION

This paper examines sand-size sediments from modern streams within the climatic and physiographic context of an undissected to transitional magmatic arc (*sensu* Dickinson, 1985) where a variety of dominantly extrusive parent rocks produce volcaniclastic sand mixed with sedimentaclastic and plutoniclastic detritus (e.g., Ingersoll, 1983). The petrographic composition of this sand with andesitic>>rhyolitic>>basaltic provenance can be used as a guide for the interpretation of volcaniclastic sand(stone)s from other volcanic progenitors (Garzanti and Andò, 2007a, 2007b; Morrone et al., 2017, 2020, 2021; Garzanti et al., 2018; Le Pera and Morrone, 2018; Dinis et al., 2019; Le Pera et al., 2021) and for the identification of (paleo)volcanic magmatic affinities (e.g., Critelli and Ingersoll, 1995) and provinces (e.g., Garzanti et al., 2002).

We focus on sand-size sediment carried by the El Rosario, San Vicente, and San Fernando rivers, draining largely within the Alisitos arc terranes (Fig. 1). In this study, sand petrography was conducted, integrating light-and heavy-minerals compositional analyses. Such an integrated approach allowed us to characterize the various components of the erosion across this oceanic arc terrane characterized by two distinct evolutionary phases, such as: (I) extensional oceanic-arc, characterized by intermediate to silicic explosive and effusive volcanism, culminating in caldera-forming silicic ignimbrite eruptions at the onset of arc rifting, and (II) rifted oceanic arc, characterized by mafic effusive and hydroclastic rocks and abundant dike swarms (e.g., Busby, 2004). The light- minerals composition of the three drainage systems has been used to verify how well sand composition reflects major tectono-morphologic provinces of the Alisitos Arc terranes in terms of petrofacies (e.g., Ingersoll, 1983). The study of the heavy-mineral assemblages is extensively used as an important tool to constrain provenance information in several sedimentary environments such as dune, beach, alluvial deposits, and rivers (e.g., Frihy, 1994; Mange and Otvos, 2005; Kasper-Zubillaga et al., 2008; Caracciolo, 2020), degree of chemical weathering (Andò et al., 2012; Tangari et al., 2021), hydraulic regimes (e.g., Cascalho and Fradique 2007; Garzanti et al., 2020), as well as intrastratal dissolution during burial diagenesis (e.g., Morton and Hallsworth, 2007; Velbel, 2007; Andò et al., 2012), added precision to identify contribution from minor sources, or input from source rocks with low Sand Generation Index (e.g., Palomares and Arribas, 1993), such as carbonate source rocks (e.g., Arribas, and Tortosa, 2003), and mixed sedimentary nappes (e.g., Vezzoli et al., 2004), that are otherwise diluted or unrecognizable using only the Q F L and Lm Lv Ls approach.

## GEOLOGICAL SETTING AND CLIMATE

Early Cretaceous rocks dominantly of intermediate-composition volcanism in the Peninsular ranges of northern Baja California produced large volumes of volcaniclastic detritus that were deposited in two basins of the Rosario segment of the Alisitos arc by both primary and reworked pyroclastic deposits (e.g., Marsaglia et al., 2016). Busby (2004) divided the Peninsular Ranges batholith into Western and Eastern belts. The Western Belt, also referred to as Alisitos Group (e.g., Busby, 2004), consists of dominantly intermediate composition volcanic and volcaniclastic rocks, and lesser mafic and silicic volcanic rocks, with abundant marine fossils, and associated hypabyssal and plutonic rocks (Silver et al., 1963; Fackler-Adams and Busby, 1998; Busby, 2004; Busby et al., 2006). Volcanic rocks are mainly Early Cretaceous andesites and andesitic breccias, rhyolites, and rhyolitic tuffs of Miocene age, and Miocene basalts (Fig. 1). The host rocks of the Eastern Belt are interpreted as continental-margin rocks and are restricted to Paleozoic-Mesozoic metasedimentary rocks of the eastern Peninsular Ranges (Busby, 2004). The Western and Eastern belts comprise a major batholith divided axially into a western gabbro to monzogranite belt and an eastern granodioritegranite belt (Silver et al., 1979; Silver and Chappal, 1988; Walawander et al., 1990). Sedimentary rocks of the Late Cretaceous-Cenozoic are dominated by marine conglomerate, shallow marine, and lesser fluvial gravel and sand and slide sheets of marine mudstone (Busby, 2004). Paleozoic to Mesozoic metasedimentary rocks are represented by phyllites, schists, metalimestones, and hornfels, varying from greenschists to amphibolite facies (Fig. 1).

In the study area, the present annual rainfall is 250 mm with an average annual temperature of 16°C and, since the Late Eocene, a variety of indicators suggest semiarid paleoclimate (e.g., Abbott et al., 1976; Peterson and Abbott, 1979). Specifically, the mean annual precipitation shows an extreme of about 207 mm at El Rosario on the Pacific coast (Bullock, 2003). In the San Fernando and San Vicente areas mean annual precipitation varies from 115 to 153 mm with the precipitation occurring predominantly in the cool season (61-91% in November-April). Warm-season precipitation, of tropical or low subtropical origin, can be extremely high but is usually very local (Bullock et al., 2005).

## SAMPLING AND METHODS

All sediment samples have been collected from active river bars with a total of 20 medium sand samples from the El Rosario, San Vicente, and San Fernando rivers analyzed for framework petrography and 13 medium to fine sand samples for heavy-mineral analyses (Fig. 1; Appendix 1). These were washed using $H_2O_2$ to remove clays and organic matter, air-dried, and sieved (using 1-phi intervals). The 0.25-0.50 mm size fraction was used to prepare thin sections and then analyzed for the petrographic composition of the medium sand. Choise of this size fraction enables the direct comparison with other studies on provenance for both modern rivers (Heins, 1993) and beach sands (Picard and McBride, 1993), and of arenites from the stratigraphic record (e.g., Weltjie, 1992; Dutta and Wheat, 1993). Moreover, this limited part of the grain-size spectrum proves to be a useful provenance tracer for both polymineralic grains and monocrystals (Blatt et al., 1980; Garzanti, 2016). Each thin section was etched and stained using hydrofluoric acid and sodium cobaltinitrite for identification of feldspar grains. A total of three hundred grains per sample were counted on each thin section using the *Gazzi-Dickinson* method (Ingersoll et al., 1984; Zuffa, 1985). Point-count raw data and recalculated point-count parameters of framework petrography are presented in Table 1 and Appendix 2, respectively. In addition to gross composition of sand (Fig. 2A, B), a specific point-count analysis of the volcanic lithic fragments group was carried out on 100 volcaniclastic grains per sample (Appendix 3). Operational categories of volcaniclastic sand-size grains, adopted during specific point-counting of this lithic fragments subgroup, are those of the pioneering paper by Dickinson (1970), recognized as Lv categories, then developed later by Zuffa (1980), Marsaglia (1991, 1993), and Marsaglia and Ingersoll (1992), and recently revised and defined as textural descriptors by Affolter and Ingersoll (2019). We have used the volcaniclastic detrital modes of the Alisitos arc river sand because of their high potential as source-sensitive lithic fragments, because their composition and textures have been used extensively to identify clastic supplies from mafic or felsic effusive or pyroclastic source rocks, and their associated sedimentary basins and geodynamic settings (Ingersoll and Cavazza, 1991; Marsaglia, 1991; Critelli and Ingersoll, 1995; Marsaglia et al., 2016). The sand-size volcaniclastic textural descriptors (e.g., Affolter and Ingersoll, 2019), used in this paper, have been summarized as follows: (1) Volcanic lithic with lathwork texture (Lvl); (2) Volcanic lithic with microlitic texture (Lvmi); (3) Volcanic lithic with vitric texture (Lvv); (4) Volcanic lithic with felsitic seriate texture (Lvfser); (5) Volcanic lithic with felsitic granular texture (Lvfgr); (6) Volcanic lithic with altered and undetermined composition (Lvalt/und). These categories are applied to epiclastic particles derived from physical weathering of volcanic terranes and not intended as lithic fragments dependent on the texture and mechanical properties of the older host rock units broken up during an eruption (e.g., Schmid, 1981; Di Capua et al., 2022). A brief description and interpretation of the main volcaniclastic sand-size-grains operational categories adopted in this study, using an optical polarizing microscope, have been defined as follows: (1) Lathwork (Lvl) and (2) Microlitic (Lvmi) volcanic lithic fragments which are glassy fragments that contain variable amounts of plagioclase, olivine, pyroxene, and opaque crystals. Fragments with lathwork texture contain some sand-size microlites and phenocrysts whereas fragments with microlitic texture contain silt-sized microlites. Lathwork particles (Lvl), as first defined by Dickinson (1970), have sand-size phenocrysts in a groundmass of glass or devitrified glass, and this texture is characteristic of provenance from basaltic and basaltic andesite lavas and pyroclastite source rocks. Microlitic texture (Lvmi) is typical of andesites, but it also commonly occurs in basalts, basaltic andesites, and phonolitic lava flows (e.g., Le Pera et al., 2021). (3) Vitric fragments (Lvv) are characterized by their lack of microlites and are defined as pumice or scoria and glass shards, but also include partially to wholly altered glass (Dickinson, 1970; Ingersoll and Cavazza, 1991; Marsaglia, 1992). Felsitic volcanic lithic fragments (Lvf) may include two types, (4) seriate and (5) granular (Dickinson, 1970; Ingersoll and Cavazza, 1991). Felsitic seriate texture is an anisometric mosaic, with a wide range of crystal sizes and shapes, composed mainly of feldspar, quartz, andor mafic minerals. Felsitic seriate texture is typical of dacites and andesites (Ingersoll and Cavazza, 1991). Felsitic granular texture consists of anhedral microcrystalline mosaics, with uniform, very fine grain size, composed mainly of feldspar and quartz and or mafic minerals. Felsitic granular texture is typical of rhyolites and dacites (Ingersoll and Cavazza, 1991). (6) Lvalt/und is a less common volcanic category of lithic fragments we used but not covered by the Dickinson (1970) categories, thus hindering any attempt to correlate texture and composition of the Lv grains with provenance input. Moreover, a size fraction of 0.25 mm to 0.063 mm was used for heavy-minerals separation by gravity settling in bromoform (density = 2.89 gr/cm$^3$ at 20°C). This separation with bromoform was performed under a fume hood - as a routine technique used traditionally by many other authors (e.g., Mange and Maurer, 1992; Arribas et al., 2000; Mange et al., 2007; Smale, 2007).

In the case of modern river sediments, the 0.25mm to 0.063 mm grain-size fraction yields the greatest range of heavy-minerals concentration (e.g., Mange-Rajetzky, 1983; Palomares et al., 1989; Morton and Smale, 1990; Garzanti et al., 2008; Garzanti et al., 2009; Garzanti et al., 2018). Magnetite grains were separated from this size fraction magnetically, using a bar magnet, while the remaining mineral groups were concentrated by multiple passes of the fraction through a Frantz Isodynamic magnetic separator to concentrate other five electromagnetic fractions (0.2, 0.5, 1.0, 1.5, and >1.5 Å), to facilitate the mineral identification (Parfenoff et al., 1970). One hundred transparent heavy minerals were counted per each electromagnetic fraction by ribbon strip counting procedure (Mange and Maurer, 1992). Petrographic identification and counting of detrital heavy species are listed in Table 2. For each magnetic class, the heavy-mineral fraction was placed on a glass slide and embedded in Canada balsam for optical observation. Surface textures of detrital grains were carefully described to evaluate the stages of weathering (unweathered, corroded, etched, deeply etched, skeletal) (Andò et al., 2012; Tangari et al. 2021). Heavy-mineral concentration was calculated as the volume percentage of total (HMC) and transparent (tHMC) heavy-minerals assemblages (Garzanti and Andò, 2007a, 2007 b; Garzanti, 2019) considering the magnetic and nonmagnetic fraction obtained using the Frantz instrument. In particular, the tHMC was used to integrate the provenance information from bulk petrography and heavy-minerals analysis (e.g., Garzanti et al., 2004, 2005, 2006). The hornblende color index (HCI) was used for tracing the average metamorphic grade of source rocks (Garzanti et al., 2004; Andò et al. 2014).

## RESULTS

### *Framework Petrography*

Sand classification was based on the main standard count of components such as quartz (Q), feldspars (F), and lithic fragments (L) (e.g., Garzanti, 2016, 2019) (Fig. 2A), and of partial detrital populations such as Qm K P (Fig. 2B), Lm Lv Ls (e.g., Ingersoll and Suczek, 1979) (Fig. 2C) to Qp Lvm Lsm (Graham et al., 1976) (Fig. 2D) which display proportions of lithic fragments of quartzose (Qp), volcanic, metavolcanic, hypabyssal (Lvm), and unstable sedimentary (Ls) and metasedimentary (Lsm) character. Moreover, a plot, Rg (granitic and gneissic rock fragments) Rv (volcanic rock fragments) Rm (metamorphic rock fragments) (Fig. 2E), combining phaneritic rock fragments (grains having crystals > 0.0625 mm) and aphanitic lithic fragments (grains having crystals < 0.0625 mm), has been considered, too. This plot allows evaluation of all information derived from a point count of medium-grained sand, recalculating both phaneritic and aphanitic lithic types using the Gazzi-Dickinson method of counting (e.g., Critelli and Le Pera, 1994; Critelli and Ingersoll, 1995).

Considering that the Lm Lv Ls ternary plot of determining aphanitic sedimentary and metasedimentary lithics (e.g., Ingersoll and Suczek, 1979) might overlook significant information within the medium-grained fraction (e.g., White et al., 2002; Garzanti, 2019), especially for the metamorphic rank of the metamorphic detrital grains (e.g., Garzanti and Vezzoli, 2003), the use of another ternary diagram (Dorsey, 1988) greatly increased the resolution of provenance reconstruction (Fig. 3A), based upon metamorphic and sedimentary aphanitic lithics. In addition, the Lvf-Lvmi-Lvl plot (Fig. 3B, C) has been considered to better identify the eroded volcanic source terranes (e.g., Marsaglia, 1991, 1992) of the Alisitos arc.

**Quartz.---**

This component occurs as single monocrystalline grains, as fine-grained polycrystalline grains, and as crystals in coarse-grained (phaneritic) rock fragments (sandstone, metamorphic, abundant plutonic rock fragments, and as phenocrysts in rarer volcanic rock fragments) (Fig. 4A-H; Fig. 5 C, D, G, H; Fig. 6A-F, H). Quartz ranges from 0.6% to 22.0 % (Table 1) of the total framework grains.

**Feldspars.---**

K-feldspar is subordinate in all samples and generally does not exceed 4.3%. Plagioclase is always more abundant than K-feldspar, and it ranges from 15.3% to 44.0% of the total framework grains (Table 1). Both K-feldspar and plagioclase occur dominantly in plutonic phanerites though plagioclase is also common as phenocrysts and embedded in volcanic lithic fragments in the amount of 3.4% (Fig. 4A-D, G, H; Fig. 5A-D, G, H; Fig. 6 A-H; Fig. 7 A-F). Secondary epidote often originates at the expense of crystal plagioclase cores.

**Lithic Fragments.---**

This category includes only fine-grained (aphanitic) fragments (Appendix 2) because the coarse-grained (phaneritic) rock fragments were not counted as rock fragments, but assigned to their respective monomineralic categories (i.e., quartz, feldspars, micas) depending on which crystal was encountered at the crosshair, according to the Gazzi-Dickinson method. However, the abundance of phaneritic rock fragments (Fig. 4 A, B; Fig. 5C, D; Fig. 6 G, H; Fig. 7 A, B, E, F) has been recalculated from the Gazzi–Dickinson database (e.g., Critelli and Le Pera, 1994). Unaltered volcanic grains were subdivided using their textural attributes into the following categories as explained in the method section. In order of decreasing abundance, they include the following categories: volcanic lithic with microlitic texture (Lvmi), with felsitic granular texture (Lvfgr), with lathwork texture (Lvl), lithic with felsitic seriate texture (Lvfser), and lithic with vitric texture (Lvv). In the latter category are included pumice grains of the El Rosario and San Vicente rivers which these range from 0.3% to 5.6% of the total framework grains (Table 1). Lvmi contain variable amounts of microlites of feldspar and ferromagnesian minerals, such as brown amphibole and biotite, opaques, and rutile, visible at high magnification (Fig. 5A-D; Fig. 6 A, B, D-F; Fig. 7 A-F). These grains range from 2.3% to 19.3% with respect to the total framework grains (Table 1).

Another volcanic category includes holocrystalline aggregates of silt-to sand-size crystals not covered by the Dickinson (1970) categories (e.g., Lvo of Marsaglia, 1993; Fig. 5E, F). These, as suggested by Marsaglia (1993) are probably fragments of glomerocrysts or holocrystalline basalt to microgabbro. Some Lvmi grains are unaltered; others show microlites of plagioclase sericitized and the glassy groundmass often oxidized or replaced by clay minerals and palagonite (Fig. 7G, H). Felsitic volcanic lithic fragments (Lvf) with granular texture are more abundant than those with seriate texture (Fig. 4G,H; Fig. 6E, F; Fig. 7A,B) with Lvfgr grains 2.3 times higher than Lvfser (Appendix 3). Lvfser are characterized by phenocrysts of quartz and brown amphibole in a glassy groundmass. Some phenocrysts less commonly are replaced by calcite. Volcanic grains with lathwork texture (Lvl) rank third in abundance of the Lv grains groups with respect to both total framework grains and in the specific point-count analysis of the only volcanic lithic fragments group carried out on 100 volcaniclastic grains (Appendix 3; Fig. 3B). They range from trace amounts (0.6%) to a maximum value of 8.3% of the total framework grains (Appendix 2). The glassy groundmass is sometimes altered to Fe-oxides or clay minerals, and the phenocrysts are made up of amphibole and plagioclase laths. Rare Lvl grains show the epidotization alteration process. Both Lvmi and rarer Lvl grains have been found also in sandstone grains (Fig. 6A, B). Volcanic lithic grains with vitric texture (Lvv) are colorless (Fig. 5G, H) and mostly altered. Some grains show vesicles filled with clay minerals and probable zeolite (Fig. 7G, H). Other Lv grains have been altered to chlorite and Fe-oxides (Lvalt, Fig. 6 C, E, F; Fig. 7C-F). This category of Lv includes trace amounts of pumice grains and shards (Lvv, Fig. 5G, H) in the sand of the El Rosario and San Vicente rivers (Table 1). Furthermore, a moderate percentage of altered and undetermined volcanic lithic grains (Appendix 3) wholly altered and thus unrecognizable or with a relict texture have been ascribed to a vesiculated hyaloclastite texture (Fig. 6C, E, F; Fig. 7C-H). Subvolcanic-hypabyssal lithic grains may be ascribed to granodiorite and tonalite clastic supply.

Sedimentary aphanitic lithic grains (Ls) are more abundant than metamorphic aphanitic lithic grains (Lm). Ls are dominated by both siliciclastic grains (siltstone+shale) and carbonate lithics (micritic, sparitic, silty-arenitic, and biomicrites limestones); metamorphic aphanitic lithic grains are mainly phyllites and minor fine-grained schists (Appendix 1; Lm, Fig. 6C, E, F; Fig. 7C, D). Single spar of calcite, occur in very low amounts (Fig. 5G, H).

The most common phaneritic rock fragments have plutonic and gneissic compositions (Fig. 4A, B; Fig. 5C, D; Fig 6G, H; Fig. 7A, B, E, F). Granodiorite and tonalite are the dominant plutonic grains derived from the Upper Cretaceous plutonic suite including granodiorite and tonalite intrusions (Fig. 1). Fe-oxides concretions and alterites have been counted, as well.

The gross composition of the river sands incorporate also results from the recognized heavy-mineral spectrum under thin section during the Gazzi-Dickinson point counting (Table 1). This is characterized by both transparent, most prevalent, and opaque minerals. The suite of transparent heavy minerals, found in the three sampled river sands, consists mainly of single crystals of green-brown and green hornblende (Fig. 4A, B ; Fig.6E, F), epidote (Fig.4G, H), titanite, and minor quantities of garnet and trace amount of tourmaline (Fig.6A, B), cordierite, pyroxene (Fig.5C, D; Fig.6H) and zircon (Table 2). Hornblende is contained also mainly in plutonic rock fragments (Fig.6G, H) and in minor metamorphic and volcanic lithic grains.

## *Modal Sand Composition*

El Rosario, San Vicente, and San Fernando rivers sands, derived from the Early Cretaceous Alisitos arc terranes (Busby, 2004; Marsaglia et al., 2016) and the Cretaceous batholith belt (Morris et al., 2019), display a restricted feldspathic lithic composition, characterizing sediments deposited along a convergent plate margin (e.g., Dickinson, 1985). These rivers carry minor feldspatho-lithic (Fl) to quartzo-litho-feldspathic (qFL) sand and dominant quartzo-feldspatho-lithic (qLF) and litho-feldspatho-quartzose (lQF) sand (Fig. 2A), with P > K-feldspar (Fig. 2B). From the Qm K P recalculation (Appendix 2; Fig. 2B), on average, plagioclase exceeds K-feldspar with a P/F ratio of 0.91. El Rosario drainage contributes more monocrystalline and zoned plagioclase grains to the river sand (e.g., Fig. 4C, D) with little changes in their proportions downstream (Appendix 2).

In the Q F L diagram (Fig. 2A), the composition of the three rivers sands seems to be homogeneous, but some changes in composition, related to the transport process can be observed. In the upstream sand of San Vicente River (SC229), the total lithics of 70% (Fig. 8A; Appendix 2) record an abrupt decrease to 42% in nearly 10 km of downstream transport (Fig. 8A). Specifically, sedimentary lithic fragments of this river sand record a decrease of 7% from the upper (km 0) to the lower reaches (km 34) of the drainage (Fig.8B). The Lvf Lvmi Lvl diagram (Fig. 3B) emphasizes the mixed proportion of microlitic, felsitic, and lathwork volcanic grains, and underlines a relative downstream decrease of the Lvl volcanic lithic grains for sand of all the three rivers. The Lvf Lvmi Lvl grains population suggests that the most durable volcanic grains (Lvmi and Lvf) preserve their abundance from the upper to the lower reaches of the drainages whereas the more labile volcanic grains (Lvl) show a discontinuous trend for both San Vicente and San Fernando rivers (Fig. 8C). On the contrary, the El Rosario River is characterized by a downstream increase of the Lvl grains that might be produced by minor tributaries input.

The volcaniclastic detritus is dominated by microlitic and felsitic grains and minor lathwork grains (Figs. 2E, 3B).

### *Heavy Minerals*

The results of grain counting of heavy-mineral analysis are listed in Table 2. The tHMC is generally defined as moderately poor ($1 \leq$ tHMC $< 2$), moderately rich ($2 \leq$ tHMC $< 5$), and rich ($5 \leq$ tHMC $< 10$). The unique difference is shown in the sample SC217 related to the San Fernando River defined as very rich ($10 \leq$ tHMC $< 20$), and the SC260 sample collected from El Rosario River reaching up an extremely rich tHMC $> 20$.

The heavy-minerals suite observed in the San Fernando, San Vicente, and El Rosario rivers system includes mainly amphibole, pyroxene, epidote, titanite, and zircon, and a minor amount of staurolite, rutile, actinolite, tourmaline, garnet, and apatite (Fig. 9A-C). The main difference in composition is shown by San Fernando river sand where minor andalusite, as well as sillimanite and kyanite, are also present. Specifically, a minor amount of sillimanite in some samples of San Vicente and kyanite in El Rosario sands respectively are also observed.

Magmatic heavy minerals predominate in El Rosario River (~ 60%) compared to San Fernando and San Vicente rivers sand (~ 50%), which are enriched in metamorphic heavy minerals ranging from 30% to 45% (Fig 10A). Metasedimentary heavy minerals are more abundant in San Fernando, reaching up to 25%, than in the San Vicente and El Rosario rivers sands where the range is between 6% and 10% (Fig 10A).

The electromagnetic Franz fraction indicates different concentrations in the heavy-mineral species (Fig. 11). Specifically, zircon, titanite, sillimanite, kyanite, andalusite, and apatite are concentrated mainly in the electromagnetic fraction > 1.5 Å and 1.5 Å, respectively. Titanite predominates in the fraction at 1.5 Å. Epidotes are concentrated in all electromagnetic fractions analyzed with a major content at 1.0 Å. In contrast amphibole and pyroxene characterize the lower magnetic fraction at 1.0 Å, 0.5 Å, and 0.2 Å. Specifically, orthopyroxene including hypersthene prevails in the 0.2 Å and 0.5 Å electromagnetic fractions. Amphibole is characterized mainly by hornblende (Fig. 9A1-3) and subordinately by actinolite and tremolite. Specifically, the San Fernando and San Vicente rivers are enriched mainly in magmatic hornblende (Hbl magmatic from 64% to 86%, as oxyhornblende and green-brown in color, Figs. 9A1-2, 10B) compared to the El Rosario River sands, where an enrichment in metamorphic hornblende occurs (Hbl Metamorphic from ~ 55% to 66%, from green to bluish green in color;, Figs. 9A3, 10B). An exception showing enrichment in metamorphic hornblende in the sample SC215 related to the San Fernando River occurs (Hbl Metamorphic ~ 64%, Figs. 9A3, 10B). The HCI index, ranges from 26 to 43 in San Fernando and from 31 to 41 in San Vicente and El Rosario rivers, respectively (Table 2). A minor amount of tremolite is observed only in some samples of San Fernando sands (SC2019, SC210, SC211 samples). Pyroxene detrital grains include mainly augite and hypersthene (Fig. 9A4-5) and low amounts of diopside (Fig. 9A6) and enstatite. These minerals exhibit low proportions in San Vicente River sands (Fig. 11). Specifically, hypersthene shows higher abundance than the augitic clinopyroxene component in El Rosario sands with the presence of spinel as inclusion. Diopside is observed only in the San Fernando River in addition to the low amount of enstatite which is detected also in the sample SC235 collected in the San Vicente River.

Most of the analyzed heavy minerals display angular and subangular morphologies (Fig. 9A1-C1) but subrounded to rounded detrital grains are also present (Fig. 9C2-5). Hornblende and pyroxene show mainly corroded to etched morphologies (Fig. 9A1, 2, 5, 6; Fig. 10C, D). Specifically, etched morphology characterizes mainly the pyroxene more than the amphibole (Fig. 10D). Unweathered morphologies of hornblende and pyroxene (mainly hypersthene, Fig. 9A4) are also often observed.

Epidote, including also minor piemontite, pistacite clinozoisite, and zoisite, was observed in San Fernando River sand. These minerals show mainly unweathered morphologies except in the San Vicente River, sands where the corroded morphologies prevail (Fig. 9B1). Epidotes with etched morphologies are observed mainly in El Rosario River sands.

Staurolite, kyanite, andalusite, and sillimanite showing prismatic habit are mainly corroded in morphologies (Fig. 9B2-3). Specifically, staurolite often exhibits the presence of mamillae on its surface (Fig. 9B3). Garnet is mainly colorless from unweathered to corroded in morphology (Fig.

9B4). Titanite is predominantly colorless with some grains yellow and pink in color (Fig. 9B5-6). This mineral shows unweathered morphology except in the San Vicente River sand where a higher corrosion degree is detected.

Zircon, rutile, and tourmaline (Fig. 9C1-6) are mainly subrounded (> 40%) with rounded grains ranging from 10 to 50% are concentrated mainly in the San Fernando River sand (Fig. 9C2-5). ZTR assemblage, showing euhedral habit, is predominant in the San Fernando River sand (Fig. 9C1; Fig. 10A). Some broken grains of zircon in the San Fernando River sands are also observed. Zircon is colorless (Fig. 9C1-2) with some pink grains observed in the San Fernando River sand, where a higher abundance of this mineral is observed.

Tourmaline, ranging from about 1% to 4%, include also yellow-brown dravite and green-bluish schörlite species (Mange and Maurer 1992; Van Loon and Mange, 2007). Schörlite is observed in El Rosario River and San Fernando sand where the dravite as well as San Vicente is also present (Fig. 9C3-4). Rutile is mainly brown in color with some grains in the shade of red and yellow in the San Fernando River sand (Fig. 9C5-6). Generally, heavy minerals show a higher degree of alteration in San Vicente, which reach 63%, than in the San Fernando and El Rosario rivers sands, where the altered grains reach mean values of 28% and 53% respectively.

## DISCUSSION

### *Baja California Source-rock Types and their Detrital Contributions*

The main sources of the El Rosario River are volcanic with subordinate sedimentary and metasedimentary and felsitic plutonic rocks such as diorite+granodiorite+tonalite.

The sand detrital modes of this river exhibit a quartzo-feldspatho-lithic (qlF) to a litho-feldspatho-quartzose (lQF) composition (Fig. 2A), as a typical characteristic of Circum Pacific volcano-plutonic sand (e.g., Garzanti, 2016, 2020). Unroofing of deeper crustal levels of the source terranes (e.g., Garzanti et al., 2021), and a higher Sand Generation Index (e.g., Palomares and Arribas, 1993) of the

Upper Cretaceous-Paleocene diorite and Upper Cretaceous granodiorite and tonalite source rocks, might provide a greater amount of monomineralic quartz (Q) and feldspar (F) grains to these sand detrital modes.

The San Vicente and San Fernando rivers, even if draining mainly sedimentary source rocks, are also dominated by a quartzo-feldspatho-lithic (qlF) to a litho-feldspatho-quartzose (lQF) composition. In more specific plots (Fig. 2B-D), the volcaniclastic supply among the three drainage rivers is better reflected by a high P/F ratio (Fig. 2B) and a cluster of the sands in the volcaniclastic field (Fig. 2C, D). San Fernando and San Vicente are dominated by siliciclastic grains such as mudstones+shale+siltstone+chert+argillite. Recalculated percentages of Ls Lm1 Lm2 parameters (Appendix 1; Fig. 3A) reveal that all the fluvial sand compositions plot on the Ls/Lm2 side of the triangular diagram and the absence of the Lm1 grains subpopulation. This triangular diagram displays that Ls show higher percentages compared to the Lm2; these latter comprise mainly phyllite and schist grains (e.g., Dorsey, 1988) (Fig 6C, E, F; Fig. 7C, D). If considering each drainage-basin sand, Ls grains prevail over Lm2, especially for San Vicente and San Fernando rivers (Fig. 3A) attesting to the significant recycling related to Upper Cretaceous-Cenozoic clastic rocks (e.g., Busby, 2004). On the other hand, the El Rosario River sand has higher Lm2 abundances (Fig. 3A) related to the erosion of Lower Cretaceous metasediments of the Alisitos arc terranes. Low-grade metamorphic lithic grains (Lm1 of Dorsey, 1988) are totally lacking in the sand of all three drainages (Fig. 3A) confirming their greatly reduced supply during sediment transport and reworking in the depositional environment (e.g., Suttner 1974; Mack 1978; Picard and McBride, 1993; Arribas et al., 2000). When differentiating among different types of sedimentary and metasedimentary source rocks (Appendix 2), sedimentary siliciclastic lithic grains prevail over carbonate lithic grains in all the sand of the three drainage basins. The results shown in the Appendix 2 provide further confirmation that El Rosario River sand is dominantly metamorphiclastic and that sedimentaclastic detritus is mainly carbonaticlastic for the San Fernando River sand and siliciclastic for the San Vicente River sand.

### *Comparison of El Rosario, San Vicente, and San Fernando Rivers Rands*

The main source rock types of the study area consist largely of volcanic, sedimentary, plutonic, and metamorphic rocks (Fig. 1). El Rosario, San Vicente, and San Fernando rivers are good examples of mixed sand deposits from a compound source (e.g., Palomares and Arribas, 1993) (Fig. 12).

The two dominant sources in the drainage basin of the El Rosario River are volcanic and sedimentary, whereas those of the San Vicente and the San Fernando are sedimentary and volcanic (Fig. 12). All the drainages are characterized by subordinate plutonic and metamorphic source rocks. Because lithic grains, both aphanitic and phaneritic, are unequivocally related to their source, the contrast between their abundance in the sand and the areal extent of the source lithology in the drainage basin, allows us to evaluate the extent to which each grain type is representative of that source (e.g., Le Pera and Arribas, 2004; Le Pera et al., 2021). The influence of differing proportions of specific bedrock types in the source area (Fig. 12) on the composition of the fluvial sand have been assessed by petrographic methods (Figs. 2-11). Sedimentary source rocks of the three drainages have a poor productivity in the carbonate and siliciclastic lithic fragments (Ls), compared with the Lv productivity. Indeed, an outcrop area of volcanic rocks of about 19.1% to 26.3% (Fig. 12) produce 77% to 68% of the total lithic population (Table 1; Fig. 2C, D, E), values comparable or equal to an outcrop area of this lithology of about 44.5% (Fig. 12). The amounts of volcanic lithic grains with felsitic and microlitic textures remain virtually unchanged throughout the river channels (Appendix 3; Fig. 3B). The relatively rapid rate of disintegration, causing comminution of lathwork volcanic (Lvl) lithic grains, can be related to the preferential widening of straight mineral boundaries of the plagioclase-plagioclase interfaces rather than sinuous mineral contacts (e.g., Le Pera and Morrone, 2020). Glass-poor microlitic lithic (Lvmi) grains, ascribed to andesitic provenance (e.g., Marsaglia, 1993) and chemically and mechanically durable felsitic (Lvf) grains, such as rhyolite and dacite fragments (Garzanti et al., 2002), record a persistent abundance from upstream reaches to the lower reaches of the rivers by virtue of their high durability during long- distance transportation (e.g., Cameron and Blatt, 1971; Cather and Folk, 1991; Smith and Lotosky, 1995).

The San Fernando and San Vicente rivers, draining mainly very low-grade Paleozoic to Mesozoic metasedimentary rocks (Fig. 1), carry quartzo-lithic sand dominated by shale and slate and siltstone and volcanic rock fragments, derived from the Alisitos arc lavas and ignimbrites (Fig. 2C, D). Other than the decrease of the Lvl volcanic grains, another marked downstream reduction is the sedimentary- grain (Ls) content of the sand of the three river systems (Appendix 2; Fig. 2C, D), although both San Vicente and the San Fernando drainage basins receive mainly clastic supplies from sedimentary and metasedimentary source rocks (Fig. 1). The Ls under representation in these fluvial sands, and their progressive reduction in less than 100 km of downstream transport, have been addressed by many studies that showed that no prolonged or intense abrasion is required for the rapid destruction of labile lithic grains (e.g., Shukis and Ethridge, 1975; Picard and McBride, 1993; Arribas et al., 2000). Moreover, dissolution during pedogenesis and intense weathering under tropical climates are other significant factors that enhance dissolution rates of sedimentary and metasedimentary particles (e.g., Johnsson, 1990; Cavazza et al., 1993; Garzanti, 2017). El Rosario carries quartz-litho-feldspathic and litho-feldspatho-quartzose sand derived mostly from the Alisitos arc terranes and minor metasedimentary rocks (Fig. 2C, D). The Lvf Lvmi Lvl diagram of Fig. 3C is a sensitive indicator of volcanic provinces and tectonic settings (e.g., Marsaglia, 1991, 1993; Critelli and Ingersoll, 1995; Critelli et al., 2002; Marsaglia et al., 2016). Andesitic provenance has microlitic-rich sand with dominant Lvmi volcanic textures (e.g, Morrone et al., 2017, 2021) and sandstones (e.g., Critelli and Ingersoll, 1995), whereas basaltic provenance has dominantly lathwork lithics (e.g., Marsaglia, 1993; Le Pera et al., 2021) with textural types of Lvl particles dominant. Moreover, felsitic volcanic lithic fragments including the two types, granular and seriate (Dickinson, 1970; Ingersoll and Cavazza, 1991) are ascribed to rhyolitic and dacitic provenances and to dacitic and andesitic provenance, respectively (Ingersoll and Cavazza, 1991). The proportions of the three sampled river sands are microlitic-rich, suggesting a prevalent detrital input from Early Cretaceous andesites and andesite breccias source rocks. El Rosario and San Fernando river sands are more shifted towards the Lvf pole (Fig. 3B), and in this case, the Lvf content could be ascribed to provenance from the Miocene rhyolite source rocks.  All three fluvial sand samples contain minor quantities of volcanic grains, with Lvl texture ascribed to a basaltic provenance. These grains having a very low preservation potential during the sediment routing system (e.g., Hatzenbuhler et al., 2022), in the case study, range from 10% to 20% and these probably have been preserved because controlled by a semiarid climate/paleoclimate of the study area (Abbott et al., 1976; Peterson and Abbott, 1979) that have not caused a significant decrease in volcanic lithic population. Moreover, few altered particles of Fe-oxides concretions and alterites could be ascribed to provenance from soil horizons (e.g., Johnsson, 1990), even if a detrital supply from altered glassy volcanic grains cannot be ruled out (e.g., Marsaglia, 1993).

### *Provenance and Weathering of Heavy Minerals*

We observed that heavy-mineral assemblages detected in San Fernando, San Vicente, and El Rosario river sands indicate a mixed provenance characterized mainly by magmatic source rocks (Fig. 10A). Specifically, the dominance of oxy-hornblende and green-brown hornblende associated with hypersthene, augitic clinopyroxene, titanite, and minor diopside suggest a provenance from andesite, rhyolite, and basalts (Fig. 10A) (e.g., Garzanti and Andò, 2007b; Garzanti et al., 2013).

A major presence of magmatic hornblende in the San Fernando and San Vicente River sands (Fig. 10B) also suggests a clear signal of provenance from magmatic rocks volcanic and plutonic, respectively. This can be related to a higher Sand Generation Index produced by the granitoid rocks, drained from the San Fernando and San Vicente Rivers respectively, from 14 to 20 times greater than metasedimentary rocks (e.g., Palomares and Arribas 1993; Caracciolo , 2020). In contrast, in the El Rosario sands, the major presence of metamorphic hornblende can be related to metasedimentary source rocks (Fig. 1).

The presence of garnet, staurolite, andalusite, kyanite, sillimanite, tremolite, and actinolite, and some epidotes (such as pistacite, zoisite, and clinozoisite), mainly in San Fernando River system, also suggests a provenance from metasedimentary and metamorphic rocks such as phyllite, schist, and gneiss (e.g., Singh et al., 2004; Garzanti et al., 2020). Staurolite generally forms in metasedimentary rocks (e.g., Mange and Morton 2007), and the presence of mamillae on its surface (Fig. 9B3) indicates a more advanced stage of weathering (Velbel et al, 1996; Andò et al., 2012). Epidote can be considered derived from the Carboniferous-Permian to Triassic metasediments (Fig. 1) or from hydrothermally altered plagioclase in mafic or felsitic source rocks (e.g., Banerjee and Gillis; 2001 Humphris and Thompson, 1978; Tangari et al., 2018).The partly magmatic provenance of the epidote is in good agreement with the point counting of light minerals which shows this mineral included mainly in plutonic rock fragments (Table 1). Furthermore, the formation during diagenetic authigenesis as suggested by Marsaglia et al.(2016) is also considered.

Epidote is mainly unweathered but shows mainly corroded and etched shapes in San Vicente and El Rosario sands, respectively, in good agreement with its lower stability during the burial diagenesis than that of garnet, staurolite, and kyanite (Morton, 1984; Morton and Hallsworth, 1999). Specifically, garnet, staurolite, and kyanite show a major degree of corrosionin the San Vicente and San Fernando sands suggesting burial depths ranging from 1100 to 1400 m (Morton, 1984; Morton and Hallsworth, 1999).

Hornblende and pyroxene commonly display a degree of corrosion (Fig. 10C, D) more shifted toward the etched morphology in the pyroxene grains (Fig. 10D) due to the diagenetic dissolution (e.g., Berner et al., 1980; Andò et al., 2012). Furthermore, the two well-developed cleavage planes in pyroxenes and amphiboles undoubtedly contribute to their vulnerability to chemical weathering. Specifically, the texture of orthopyroxene and clinopyroxene, more shifted towards the etched morphologies (Fig. 9A5-6), are in good agreement with their highly unstable nature in sandstones, being more stable only than olivine (e.g., Pettijohn, 1975; Morton, 1984). Furthermore, these minerals become depleted more rapidly than amphibole and epidote during burial, and by the advanced development of grain surface corrosion textures in the shallow subsurface (Turner and Morton, 2007). Predominant subrounded ultrastable zircon, tourmaline, and rutile (ZTR), also including some rounded surface textures (Fig. 9C2-5), suggest mechanical abrasion during reworking processes and/or long-distance transport related to the sedimentary and metasedimentary source rocks (e.g., Knox et al., 2007; Garzanti et al.,2013;2017; Cascalho, 2019; Zoleikhaei et al., 2021). Nonetheless, the presence of ZTR with euhedral habits, mainly zircon observed in the San Fernando River, can be defined as likely to be of first-cycle origin (Knox et al., 2007) suggesting a provenance from igneous source rocks (e.g., Wilson, 1981). Specifically, zircon with typical euhedral and prismatic habit (Fig. 9C1) showing pink color has been detected in the San Fernando River. This mineral suggests a magmatic provenance (i.e., granite and granodiorite) as observed in other river sands (Brondi et al. 1972; Wilson 1981). Likewise, the magmatic provenance of tourmaline and rutile has been widely investigated (e.g., Mehinold 2010; Yücel-Öztürk et al., 2015; Beyranvand et al., 2021). In particular, these minerals are widely detected in many igneous and plutonic rocks such as granite (e.g., Povondra et al., 1998; Carruzzo et al., 2006; Clarke and Carruzzo, 2007; Mehinold 2010; Salata , 2014; Kotowski et al., 2020; Naidu et al., 2020). Specifically, tourmaline detected in igneous rocks is often enriched in schörlite and dravite species (e.g., Henry et al 2011; Salata , 2014; Kotowski et al., 2020), in agreement with the type of tourmaline detected in the river sand analyzed in the study area.

### *Comparison to Other Magmatic Arcs and Mafic vs. Intermediate-Felsic Volcanic Provenances*

The studied modern volcaniclastic sand of the El Rosario, San Vicente, and San Fernando rivers exhibits a composition data set similar to that of both Cenozoic magmatic arc (Marsaglia and Ingersoll, 1992) and Rio Grande Rift sand (Marsaglia, 1991) (Fig. 3C). In Fig. 3C we have plotted mean Lvf Lvmi Lvl values for Lower Cretaceous Alisitos oceanic arc, separating between the marine Rio Del Rosario measured section and the subaerial to the marine measured section at Arroyo San Fernando of the arc (Marsaglia et al., 2016). The Rio Del Rosario measured section mean falls along the line dividing the *felsic* and the *mixed petrofacies*, whereas the Arroyo San Fernando section mean plots in the mixed petrofacies we called *mixed*. The higher proportion of fragments with Lvf texture of the Rio Del Rosario section with respect to the San Fernando section might be related to a very thick exposure of a silicic ignimbrite widespread only in the Rio El Rosario section of the Alisitos Group (Busby et al., 2006; Marsaglia et al., 2016). Both the Rio El Rosario and San Fernando measured sections contain nearly equal proportions of grains with lathwork texture (Lvl), consistent with a main source of more mafic composition, that which in the two studied sections are represented by basaltic blocks and sills (Marsaglia et al., 2016). The El Rosario and San Fernando rivers sands, largely reworked from older Alisitos Group volcaniclastic rock outcrops (Marsaglia et al., 2016), plot in the intermediate field of the Lvf Lvmi Lvl space, evidencing a decrease from a maximum value of 16% to a minimum value of 10% of the Lvl lithic grains (Fig. 3C), thus confirming their low mechanical and/or chemical durability during the sediment dispersal by grain fracturing (e.g., Le Pera and Morrone, 2020). Conversely, an increase of the volcaniclastic sandy particles with Lvmi and Lvf textures of the studied modern sands with respect to Alisitos Group volcaniclastic rocks (Fig. 3C) can be attributed to a transport process of rounding through abrasion of these volcaniclastic grains (e.g., Le Pera and Morrone, 2020). Specifically, the abundance of more brittle grains such as those with Lvl textures seems to be controlled by a comminution process that splinters them into smaller grains whereas that of volcaniclastic grains with Lvf and Lvmi textures are influenced mainly by rounding through abrasion (e.g., Cather and Folk, 1991; Le Pera and Morrone, 2020; Le Pera et al., 2021). The main mineralogical signatures of sand generated in the El Rosario, San Vicente, and San Fernando catchments reflect erosion of the lithological units exposed as described in Busby (2004), such as the (I) extensional oceanic arc, characterized by intermediate to silicic explosive and effusive volcanism, culminating in caldera-forming silicic ignimbrite eruptions at the onset of arc rifting, and (II) rifted oceanic arc, characterized by mafic effusive and hydroclastic rocks and abundant dike swarms. The contribution of volcaniclastic supply and the varying proportions of Lvf Lvmi Lvl sand detrital modes of the three studied rivers attest to provenance from largely intermediate and silicic effusive volcanism arc terranes and from minor mafic effusive rocks, whereas compositional signatures from hydroclastic rocks are absent.

A dominant provenance from Early Cretaceous andesites and with subordinate supply of felsitic sand from the Miocene rhyolites and rhyolitic tuff has been recorded by the El Rosario, San Fernando, and San Vicente river sands, even if in this case it has not been possible to confidently discriminate between paleovolcanic and neovolcanic particles (e.g., Garzanti et al., 2013) but only between Lvmi and Lvf textures.

The mean composition of the three studied river s of the Baja California roughly correlates with a dominant *andesitic* provenance in the intermediate petrofacies field of Figure 3C, where have been plotted other arc-related sand and sandstone compositions such as those recovered on Leg 64 (Gulf of California; Marsaglia, 1991), Leg 126 (Izu-Bonin Arc; Marsaglia, 1992) of the Deep Sea Drilling Project, of the Cenozoic Magmatic Arc (e.g., Marsaglia and Ingersoll, 1992), and of the Miocene deep-marine turbidite sandstones of the Topanga Group (e.g., Critelli and Ingersoll, 1995).

The El Rosario, San Fernando, and San Vicente rivers, draining an orogenic andesitic arc (Busby, 2004), contain abundant loose monocrystals of plagioclase and a lower content of rock fragments (Fig. 2A, B). This crystal-rich andesiticlastic sand may account for an epiclastic origin of the detritus that is not a product deposited penecontemporaneously with active volcanism characterized by higher contents of volcanogenic rock fragments that reflect syneruptive and intereruptive volcanism (e.g., Smith and Lotosky, 1995). The Lvf Lvmi Lvl diagram adequately represents the extrusive source rocks in the source area of the drainages characterized by Early Cretaceous andesites and Miocene basalts+rhyolites+rhyolitic tuffs (Fig. 3C). These sand detrital modes, enclosed in the Intermediate petrofacies field in the Lvf Lvmi Lvl space, are comparable with those of Cenozoic magmatic-arc related terranes (e.g., Marsaglia and Ingersoll, 1992), Plio-Pleistocene Gulf of California Leg 64 sand (e.g., Marsaglia, 1991), Quaternary sand of the Izu-Bonin Leg 126 (Marsaglia 1992) and of the Miocene deep-marine sandstone of the Topanga Group (e.g., Critelli and Ingersoll, 1995). The higher volcanic lithic content of lathwork (Lvl) grains in the Izu-Bonin sand suggest that the more mafic component is probably derived from intrarift mafic volcanic centers supplying sediment to the Sumisu Rift via turbidity currents and gravity flows (e.g., Marsaglia, 1991). Lesser Lvl grain types of the three studied rivers could suggest that these labile volcanic textures (e.g., Le Pera and Morrone, 2020) are affected by stream transport before transport into deeper water. The Topanga Group sandstones suggest a principal volcanic provenance from mafic lavas such as basalts and basaltic andesites lava flows with minimal diagenetic alteration (Critelli and Ingersoll, 1995). Offshore Plio-Pleistocene sand of the Gulf of California (Leg 64; Marsaglia, 1991) and the Cenozoic magmatic-arc sand (e.g., Marsaglia and Ingersoll, 1992) are more shifted towards the mean values of the three sampled river sands. The andesitic source terranes of Baja California provide predominantly microlitic volcanic lithic fragments to the offshore sand, but the Plio-Pleistocene offshore sand is more depleted in the felsitic lithic fragments (Marsaglia, 1991) with respect to the modern Baja California river sands. Moreover, Cenozoic magmatic-arc sands (e.g., Marsaglia and Ingersoll, 1992), reflecting a spectrum of volcanic rocks ranging from tholeiitic basalts to calc-alkaline basalts, andesites and dacites, have higher microlitic proportions and minor amounts of felsitic and lathwork proportions (Fig. 3C). Moreover, glass color of volcanic grains, as a proxy for composition in intraoceanic magmatic-arc basin fills were detailed in Marsaglia (1992) and later by Marsaglia and Devaney (1995). This latter points out that except for tachylitic glass, color can be lost via diagenetic overprinting in older successions limiting interpretations, thus emphasizing the need to rely on other textural evidence that may better survive diagenesis such as Lvf, Lvmi, Lvl grains, as also documented by Marsaglia and Tazaki (1992).

### *The Recycling Problem*

Signals of recycling of grains from sedimentary and metasedimentary source rocks (Fig. 1) are evident in the composition of sands from the El Rosario, San Vicente, and San Fernando rivers.

The difficulties involved in the reconstruction of the provenance of the studied Baja California river sands are related to a complex geodynamic setting including a mixture of detrital sources supplying both first-cycle and multicycle detritus. Nonetheless, during the petrographic analysis, useful textural parameters helped in provenance diagnosis and allowed us to add some details in evaluating a distinction between first-cycle detritus as opposed to polycyclic origin (e.g., Blatt, 1967; Zuffa, 1987). In addition to the application of the criteria listed by Zuffa (1987), such as main types of carbonates (paleo-CE or neo-CI), and paleovolcanic (V1) or neovolcanic (V2a, V2b, V3 and V4) sand particle compositions, we also suggest consideration of the roundness of the detrital sandy particles as an integral part of the provenance analysis, as suggested by Garzanti (2017), to infer recycling. Indeed, hard volcanic lithic grains such as Lvf Lvmi and Lvl (Fig. 4G, H; Fig. 5A-D, G, H; Fig.6A, B, D, F; Fig. 7A-F) and Lvo (Fig. 5E, F), are very well rounded with a texture not sufficient to establish that most of this volcaniclastic detritus is of first-cycle origin (Garzanti, 2017). The high roundness of the Baja California sandy particles is observed to be also important on hard heavy minerals such as zircon, tourmaline, and rutile (Fig. 9C). Specifically, in Fig. 9C it is clear to distinguish between a sharp euhedral crystal of zircon (Fig. 9C1), probably magmatic in origin, and a very well-rounded clast of polycyclic origin (Fig. 9C2), between a subrounded clast of tourmaline (Fig. 9C3) and of a very well-rounded clast of the same mineral (Fig. 9C4), and between a more elongated crystal of rutile (Fig. 9C5) and a more rounded clast of the same heavy species (Fig. 9C6). In this case, we suggest observing the roundness attained by the heavy-mineral assemblage of ultrastable species such as zircon+tourmaline+rutile (the ZTR index of Hubert, 1962) beyond the composition and/or color (Mange and Wright, 2007; Andò et al.,2012) and the chemical composition (e.g., Morton and Chenery, 2009; Meinhold, 2010; Wotzlaw et al., 2011; Salata, 2014). Therefore, the concentration index of transparent HM, combined with the suite of HM observed, confirms a multiple cycle of weathering and recycling in the sedimentary system.

**CONCLUSIONS**

The present study focused on modern river sands draining largely within the Alisitos arc terranes in Baja California. Because of the semiarid climate since Late Eocene time, the modern fluvial sand detrital modes are consistent with a provenance from a mixture of sedimentary, volcanic, plutonic, and metamorphic source rocks. Provenance terranes from the fluvial sand detrital modes of the study area are defined by valuable source-rock indicators such as rock fragments, both aphanitic and phaneritic, and source-sensitive heavy minerals. El Rosario is characterized by a dominance of volcanic-rock exposure. On the other hand, although Paleozoic to Mesozoic-Tertiary sedimentary and metasedimentary rocks represent most exposure area in the San Vicente and San Fernando rivers, quartzo-feldspatho-lithic (qLF) and litho-feldspatho-quartzose (lQF) sand detrital modes dominate the framework composition. This suggests a dominant provenance from the Cretaceous Alisitos arc terranes generated from an undissected to a transitional magmatic arc. Prevalence of andesitic to rhyolitic detritus from the Cretaceous-Miocene Alisitos Group is indicated by the high content of Lvmi and Lvf paleovolcanic grains whereas minor Lvl textures were plausibly shed from the Tertiary to Quaternary basalts. The volcaniclastic modern sediment flux of the three rivers is mainly paleovolcanic and is derived mainly from erosion of the extensional phase of the oceanic Alisitos arc terranes characterized by intermediate to silicic explosive and effusive volcanism, culminating in caldera-forming eruptions of silicic ignimbrite. In contrast , the rifted oceanic arc phase terranes, characterized by mafic effusive and hydroclastic rocks and abundant dike swarms, contain less abundant volcaniclastic detritus, probably because of a limited mechanical and chemical durability of the mafic and glass-rich volcanic rock fragments.

Considering the relative abundance of framework petrography, sandy grains recycled from the Upper Cretaceous to Tertiary sedimentary rocks are less significant with respect to the volcaniclastic detritus whereas the ZTR index of the heavy-minerals modes, coupled with their subrounded to rounded grain surface texture, indicates a recycling process from the sedimentary source rocks, adding precision to identification of the contribution from sources with low Sand Generation Index such as those drained by the three Baja California rivers.

The transparent heavy-mineral assemblages are in good agreement with a mixed provenance characterized mainly by magmatic, primarily volcanic (andesite, rhyolite, and basalt) and secondarily plutonic (granitoid rocks) source rocks detected through analysis of the framework petrography, based on primary parameters such as quartzose, feldspathic and lithic grains (QFL) and among proportions of diverse aphanitic and phaneritic rock fragments (Lm Lv LS and Rg Rv Rm). Specifically, heavy-mineral abundance and weathering textures in San Fernando and San Vincente river sands match predominant volcanic bedrock lithologies and El Rosario sedimentary and metasedimentary source rocks. The presence of angular to very angular surface textures of some heavy minerals suggests that mechanical weathering could directly affect the magmatic-arc terranes. The corroded and etched morphologies of the heavy minerals  suggest that more labile species, such as amphibole and pyroxenes, still show inherited diagenetic dissolution features from the Mesozoic volcanoclastic successions and by further chemical weathering processes occurring in a paleo and current semiarid climate. Therefore, the use of both light-mineral and heavy detrital mineralogy in sandstone petrological studies should be considered if they are to interpret ancient orogenic petrofacies provenances successfully.

**Acknowledgments**

We are very grateful to Prof. Salvatore Critelli, for the collection of the river-sand samples and for the suggestion and discussion of the various aspects of the study area. We are grateful to Prof. Josè Arribas, whose ideas were important to the methodological conception of this work. Heavy-minerals separation, from the sand bulk samples, using heavy-liquid and magnetic separation through the Frantz isodynamic separator, was performed in the Facultad de Ciencias Geológicas of the Universidad Complutense de Madrid (Spain) under the supervision of Prof. José Arribas. We thank Dr. Daniele Cirillo for his helpful contribution to statistical analysis on the GIS platform. We thank Editor Prof. Kathleen M. Marsaglia and Associate editor Prof. Devon Orme of The Journal of

Sedimentary Research, for their thorough revision, and Prof. Timothy F. Lawton, Prof. Warren Dickinson, and anonymous reviewers for their constructive criticism and detailed revisions, which have significantly improved this manuscript.

## REFERENCES

Abbott, P.L., Minch, J.A., and Peterson, G.L., 1976, Pre-Holocene paleosoil south of Tijuana, Baja California, Mexico: Journal of Sedimentary Petrology, v. 46, p. 355-361

Affolter, M.D., and Ingersoll, R.V., 2019, Quantitative analysis of volcanic lithic fragments: Journal of Sedimentary Research, v. 89, p. 479–486.

Andò, S., Garzanti, E., Padoan, M., and Limonta, M., 2012, Corrosion of heavy minerals during weathering and diagenesis: a catalog for optical analysis: Sedimentary Geology, v. 280, p. 165–178.

Andò, S., Morton, A., and Garzanti, E., 2014, Metamorphic grade of source rocks revealed by chemical fingerprints of detrital amphibole and garnet *in* Scott, R.A., Smyth, H.R., Morton, A.C., Richardson, N.,eds., Sediment Provenance Studies in Hydrocarbon Exploration and Production: Geological Society, London, Special Publications, v. 386, p. 351-371.

Arribas, J., and Tortosa, A., 2003, Detrital modes in sedimenticlastic sand from low-order streams in the Iberian Range, Spain: the potential for sand generation by different sedimentary rocks: Sedimentary Geology, v. 159, p. 275– 303.

Arribas, J., Critelli, S., Le Pera, E., and Tortosa, A., 2000, Composition of modern stream sand derived from a mixture of sedimentary and metamorphic source rocks (Henares River, Central Spain): Sedimentary Geology, v. 133, p. 27-48.

Banerjee, N.R., and Gillis, K.M., 2001, Hydrodrothermal alteration in a modern suprasubduction zone: The Tonga forearc crust: Journal of Geophysical Research, v. 106, p.737-750.

Berner, R.A., Sjöberg, E.L., Velbel, M.A., and Krom, M.D., 1980, Dissolution of pyroxenes and amphiboles during weathering: Science, v. 207, p. 1205–1206.

Beyranvand, D.R., Ardalan, A.A., Farhadinejad, T., and Arian, M.A., 2021, Petrography and mineral chemistry of tourmaline in Molla Taleb Granitoid, Northeat of Aligudarz(Lorestan Province): Revista Geoaraguaia, v. 11, p. 55-76.

Blatt, H., 1967, Provenance of determinations and recycling of sediments: Journal of Sedimentary Petrology, v. 37, p. 1031-1044.

Blatt, H., Middleton, G. and Murray, R. 1980, Origin of Sedimentary Rocks 2nd Edition: Prentice-Hall, Englewood Cliffs, NJ, 782 p.

Brondi, A., Ferretti, O., and Locardi, E., 1972, Sulla provenienza dei diversi tipi di zircone e monazite contenuti nei sedimenti fluviali della Calabria: Società Italiana di Mineralogia e Petrologia Rendiconti, v. 28, p. 31-52.

Bullock, S.H., 2003, Seasonality, spatial coherence and history of precipitation in desert region of the Baja California peninsula: Journal of Arid Environments, v. 53, p. 169-182.

Bullock, S.H., Martijena, N.E., Webb, R.H., and Turner, R.M., 2005, Twentieth century demographic changes in Cirio and Cardón, in Baja California, México: Journal of Biogeography, v. 32, p. 127-143.

Busby, C., 2004, Continental growth at convergent margins facing large ocean basins: a case study from Mesozoic convergent-margin basins of Baja California, Mexico: Tectonophysics, v. 392, p. 241–277.

Busby, C., Fackler-Adams, B.N., Matinson, J., and Deoreo, S., 2006, View of an intact oceani arc, from surficial to mesozonal levels: Cretaceous Alisitos Arc, Baja California: Journal of Volcanology and Geothermal Research, v. 149, p. 1–46.

Cameron, K.L., and Blatt, H., 1971, Durabilities of sand-size schist and “volcanic” rock fragments during fluvial transport, Elk Creek, Black Hills, South Dakota: Journal of Sedimentary

Petrology, v. 41, p. 565–576.

Caracciolo, L., 2020, Sediment generation and sediment routing systems from a quantitative provenance analysis perspective: Review, application and future development. Earth-Science Reviews, v. 207, no.103226.

Carruzzo, S., Clarke, D.B., and Pelrine, K., 2006, Texture, composition, and origin of rutile in the South Mountain Batholith, Nova Scotia: The Canadian Mineralogist, v. 44, p. 715-729.

Cascalho, S., and Fradique, C., 2007, The Sources and hydraulic sorting of heavy minerals on the northern portuguese continental margin, *in* Mange, M.A., and Wright, D.T., eds., Heavy Minerals in Use: Elsevier, Developments in Sedimentology, v.58, p.75-107.

Cascalho, J., 2019, Provenance of Heavy Minerals: A Case Study from the WNW Portugues Continental Margin: Minerals, v. 9,p. 1-33.

Cather, S.M., and Folk R.L., 1991, Pre-diagenetic sedimentary fractionation of andesitic detritus in a semiarid climate: an example from the Eocene Datil group, New Mexico, *in* Fisher, R.V., and Smith, G.A., eds., Sedimentation in Volcanic Settings: SEPM, (Society for Sedimentary Geology) Special Paper45, p. 211-226.

Cavazza, W., Zuffa, G.G., Camporesi, C., and Ferretti, C., 1993, Sedimentary recycling in a temperate climate drainage basin (Senio River, north-central Italy): composition of source rock, soil profiles, and fluvial deposits, *in* Johnsson, M.J., and Basu, A., eds., Processes Controlling the Composition of Clastic Sediments: Geological Society of America, Special Paper 284, p. 247–261.

Clarke, D.B., and Carruzzo, S., 2007, Assimilation of country-rock ilmenite and rutile in the South Mountain Batholith, Nova Scotia, Canada: The Canadian Mineralogist, v. 45, p. 31-42.

Critelli, S., and Ingersoll, R.V., 1995, Interpretation of neovolcanic vs. palaeovolcanic sand grains: an example from Miocene deep-marine sandstone of the Topanga Group (southern California): Sedimentology, v. 42, p. 783–804.

Critelli, S., and Le Pera, E., 1994, Detrital modes and provenance of Miocene sandstones and modern sands of the southern Apennines thrust-top basins (Italy): Journal of Sedimentary Research, v. A64, p. 824-835.

Critelli, S., Le Pera, E., and Ingersoll, R.V., 1997, The effects of source lithology, transport, deposition and sampling scale on the composition of southern California sand: Sedimentology, v. 44, p. 653–671.

Critelli, S., Marsaglia, K.M., and Busby, C.J., 2002, Tectonic history of a Jurassic backarc-basin sequence (the Gran Cañon Formation, Cedros Island, Mexico), based on compositional modes of tuffaceous deposits: Geological Society of America, Bulletin, v. 114, p. 515–527.

Critelli, S., Arribas, J., Le Pera, E., Tortosa, A., Marsaglia, K.M., and Latter, K.L., 2003, The recycled orogenic sand provenance from an uplifted thrust belt, Betic Cordillera, southern Spain: Journal of Sedimentary Research, v. 73, p. 72–81.

De Rosa, R., Zuffa, G.G., Taira, A., and Leggett, J.K., 1986, Petrography of trench sands from the Nankai Trough, southwest Japan: implications for long-distance turbidite transportation: Geological Magazine, v. 123, p. 477–486.

Di Capua, A., De Rosa, R., Kereszturi, G., Le Pera, E., Rosi, M. and Watt, S.F.L., 2022, From volcanoes to sedimentary system *in* Di Capua, A., De Rosa, R., Kereszturi, G., Le Pera, E., Rosi, M. and Watt, S.F.L., eds., Volcanic Processes in the Sedimentary Record: When Volcanoes Meet the Environment: Geological Society of London, Special Publication 520, p. 11–27. https://doi.org/10.1144/SP520-2021-201

Dickinson, W.R., 1970, Interpreting detrital modes of graywacke and arkose: Journal of Sedimentary Petrology, v. 40, p. 695–707.

Dickinson, W.R., 1985, Provenance relations from detrital modes of sandstones, *in* Zuffa, G.G., ed., Provenance of Arenites: NATO Advanced Science Institutes, Series, C-148, p. 333–362.

Dinis, P.A., Pinto, M.C., Rocha, F.T., and Garzanti, E., 2019, Detrital record of the denudation of volcanic islands under sub-tropical climate (Cape Verde): Geochemistry, v. 79, p. 235–246

Dorsey, R.J., 1988, Provenance evolution and unroofing history of a modern arc–continent collision: evidence from petrography of Plio–Pleistocene sandstones, eastern Taiwan: Journal of Sedimentary Petrology, v. 58, p. 208–218.

Dutta, P.K., and Wheat, R.W., 1993, Climatic and tectonic control on sandstone composition in the Permo-Trias Sydney foreland basin, eastern Australia, *in* Johnsson, M.J., and Basu, A., eds., Processes Controlling the Composition of Clastic Sediments: Geological Society of America, Special Paper 284, p. 187–202.

Fackler-Adams, B.N., and Busby, C.J., 1998, Structural and stratigraphic evolution of extensional oceanic arcs: Geology, v. 26, p. 735–738.

Frihy, O.E., 1994, Discrimination of accreted and eroded coasts using heavy mineral composition of the Nile Delta beach sands, Egypt: Sedimentology, v. 41, p. 905–912.

Garzanti, E., 2016, From static to dynamic provenance analysis—sedimentary petrology upgraded: Sedimentary Geology, v. 336, p. 3–13.

Garzanti, E., 2017, The maturity myth in sedimentology and provenance analysis: Journal of Sedimentary Research, v. 87, p. 353–365.

Garzanti, E., 2019, Petrographic classification of sand and sandstone: Earth-Science Reviews, v. 192, p. 545–563.

Garzanti, E., and Andò, S., 2007a, Heavy mineral concentration in modern sands: implications for provenance interpretation, *in* Mange, M.A., and Wright, D.T., eds., Heavy Minerals in Use: Elsevier, Developments in Sedimentology, v. 58, p. 517-545.

Garzanti, E., and Andò, S., 2007b, Plate tectonics and heavy mineral suites of modern sands, *in* Mange, M.A., and Wright, D.T., eds., Heavy Minerals in Use: Elsevier, Developments in Sedimentology, v. 58, pp. 741–763.

Garzanti, E., and Vezzoli, G., 2003, A classification of metamorphic grains in sands based on their composition and grade: Journal of Sedimentary Research, v. 73, p. 830–837.

Garzanti, E., Canclini, S., Moretti Foggia, F., and Petrella, N., 2002, Unravelling magmatic and orogenic provenances in modern sands: The back-arc side of the Apennine thrust-belt (Italy): Journal of Sedimentary Research, v. 72, p. 2–17.

Garzanti, E., Vezzoli, G., Lombardo, B., Andò, S., Mauri, E., Monguzzi, S., and Russo, M., 2004, Collision orogen provenance (Western and Central Alps): detrital signatures and unroofing trends: The Journal of Geology, v. 112, p. 145–164.

Garzanti, E., Vezzoli, G., Andò, S., Paparella, P., Clift, P.D., 2005, Petrology of Indus River sands: a key to interpret erosion history of the Western Himalayan Syntaxis: Earth and Planetary Science Letters, v. 229, p. 287–302.

Garzanti, E., Andò, S., Vezzoli, G., Ali Abdel Megid, A., and EL Kammar, A., 2006, Petrology of Nile River sands (Ethiopia and Sudan): sediment budgets and erosion patterns: Earth and Planetary Science Letters, v. 252, p. 327–341.

Garzanti, E., Andò, S., and Vezzoli, G., 2008, Settling-equivalence of detrital minerals and grain-size dependence of sediment composition: Earth and Planetary Science Letters, v. 273, p. 138–151.

Garzanti, E., Andò, S., and Vezzoli, G., 2009, Grain-size dependence of sediment composition and environmental bias in provenance studies: Earth and Planetary Science Letters, v. 277, p. 422–432.

Garzanti, E., Limonta, M., Resentini, A., Bandopadhyay, P.C., Najman, Y., Andò, S., and Vezzoli, G., 2013, Sediment recycling at convergent plate margins (Indo-Burman Ranges and Andaman–Nicobar Ridge): Earth-Science Reviews, v.123, p.113–132.

Garzanti, E., Vermeesch, P., Rittner, M., and Simmons, M., 2017, The zircon story of the Nile: Time-structure maps of source rocks and discontinuous propagation of detrital signals: Basin Research, v. 30, p. 1098-1117.

Garzanti, E., Limonta, M., Vezzoli, G., An, W., Wang, J., Hu, X., Ingersoll, R.V., Lawton, T.F., and Graham, S.A., 2018, Petrology and multimineral fingerprinting of modern sand generated from a dissected magmatic arc (Lhasa River, Tibet), *in* Ingersoll, R.V., Lawton, T.F., and Graham, S.A., eds., Tectonics, Sedimentary Basins, and Provenance: A Celebration of the Career of William R. Dickinson: Geological Society of America, 540, p. 197-221.

Garzanti, E., Andò, S., and Vezzoli, G., 2020, Provenance of cenozoic Indus fan sediments (IODP sites u1456 and u1457): Journal of Sedimentary Research, v. 90, p. 114-1127.

Garzanti, E., Capaldi, T., Vezzoli, G., Limonta, M. and Sosa, N., 2021, Transcontinental retroarc sediment routing controlled by subduction geometry and climate change (Central and Southern Andes, Argentina): Basin Research, v. 33, p. 3406–3437.

Graham, S.A., Ingersoll, R.V., and Dickinson, W.R., 1976, Common provenance for lithic grains in Carboniferous sandstones from Ouachita Mountains and Black Warrior Basin: Journal of Sedimentary Research, v. 46, p. 620-632.

Hatzenbühler, D., Caracciolo L., Weltje, G.J., Piraquive, A., and Regelous, M., 2022, Lithologic, geomorphic, and climatic controls on sand generation from volcanic rocks in the Sierra Nevada de Santa Marta massif (NE Colombia): Sedimentary Geology, v. 429, no. 106076.

Henry, D.J., Novák, M., Hawthorne, F.C., Ertl, A., Dutrow, B.L., Uher, P., and Pezzotta, F., 2011, Nomenclature of the tourmaline-supergroup minerals: American Mineralogist, v. 96, p. 895–913.

Heins, W.A., 1993, Source rock texture versus climate and topography as controls on the composition of modern, plutoniclastic sand, *in* Johnsson, and M.J., Basu, A., eds., Processes Controlling the Composition of Clastic Sediments: Geological Society of America, Special Paper, 284, p. 135–146.

Hubert, J.F., 1962, A zircon–tourmaline–rutile maturity index and the interdependence of the composition of heavy minerals assemblages with the gross composition and texture of sandstones: Journal of Sedimentary Petrology, v. 32, p. 440–450.

Humphris, S.E., and Thompson, G.,1978, Hydrothermal alteration of oceanic basalts by seawater, Geochimimica et Cosmochimica Acta: v. 42, p. 107–125.

Ingersoll, R.V., 1983, Petrofacies and provenance of late Mesozoic forearc basin, northern and central California: American Association of Petroleum Geologists, Bulletin, v. 67, p. 1125–1142.

Ingersoll, R.V., and Cavazza, W., 1991, Reconstruction of Oligo–Miocene volcaniclastic dispersal patterns in north-central New Mexico using sandstone petrofacies, *in* Fisher, R.V., and Smith, G.A., eds., Sedimentation in Volcanic Settings: SEPM (Society for Sedimentary Geology), Special Publication 45, p. 227–236.

Ingersoll, R.V., and Suczek, C.A. 1979, Petrology and provenance of Neogene sand from Nicobar and Bengal Fans, DSDP sites 21 and 218: Journal of Sedimentary Petrology, v. 49, p. 1217-1228.

Ingersoll , R.V.,Bullard , T.F., Ford, R.L., Grimm , J.P., Pickle , J.D., and Sares , S.W., 1984, The effect of grain size on detrital modes: A test of the Gazzi-Dickinson point-counting method: Journal of Sedimentary Petrology, v. 54, p. 103–116.

Johnsson, M.J., 1990, Overlooked sedimentary particles from tropical weathering environments: Geology, v. 18, p. 107-110.

Kasper-Zubillaga, J.J., Carranza-Edwards, A., and Morton-Bermea, O., 2008, Heavy Minerals and Rare Earth Elements in Coastal and Inland Dune Sands of El Vizcaino Desert, Baja California Peninsula, Mexico: Marine Georesources and Geotechnology, v. 26, p. 172-188.

Knox, R.W.O'B., Franks, S.G., and Cocker, J.D., 2007, Stratigraphic evolution of heavy-mineral provenance signatures in the sandstones of the Wajid Group (Cambrian to Permian), southwestern Saudi Arabia: GeoArabia, v. 12, p. 65-96

Kotowski, J., Nejbert, K., and Olszewska-Nejbert, D., 2020, Tourmalines as a tool in provenance studies of terrigenous material in Extra-Carpathian Albian (Uppermost Lower Cretaceous) sands of Miechów Synclinorium, Southern Poland: Minerals, v. 10, p. 1-28.

Le Pera, E., and Arribas, J., 2004, Sand composition in an Iberian passive-margin fluvial course: Sedimentary Geology, v. 171, p. 261-281.

Le Pera, E., and Morrone, C., 2018, Heavy minerals distribution and provenance in modern beach sands of Campania, Italy: Società Geologica Italiana, Rendiconti Online, v. 45, p. 136–140.

Le Pera, E., and Morrone, C., 2020, The use of mineral interfaces in sand-sized volcanic rock fragments to infer mechanical durability: Journal of Palaeogeography, v. 9, p. 1–26.

Le Pera, E., Morrone, C., Arribas, J., Arribas, M.E., Ancochea, E., and Huertas, M.J., 2021, Petrography and provenance of beach sands from volcanic oceanic islands: Cabo Verde, Atlantic Ocean: Journal of Sedimentary Research, v. 91, p. 92–115.

Mack, G.H., 1978, The survivability of labile light-mineral grains in fluvial, aeolian and littoral marine environments: the Permian Cutler and Cedar Mesa Formations, Moab, Utah: Sedimentology, v. 25, p. 587–604.

Mange-Rajetzky, M.A., 1983, Sediment dispersal from source to shelf on an active continental margin, S. Turkey: Marine Geology, v. 52, p. 1–26.

Mange, M.A., and Maurer, H.F.W., 1992, Heavy Minerals in Colour: Chapman and Hall, London, 147 p.

Mange, M.A., and Morton, A.C., 2007, Geochemistry of heavy minerals, *in* Mange, M.A., Wright, D.T. eds., Heavy Minerals in Use: Elsevier, Developments in Sedimentology, v. 58, p. 345–391.

Mange, M.A., and Otvos, E. G., 2005, Gulf coastal plain evolution in West Louisiana: Heavy mineral provenance and Pleistocene alluvial chronology: Sedimentary Geology, v. 182, p. 29–57.

Mange, M.A., and Wright D.T., 2007, High resolution heavy mineral analysis (HRHMA): a brief summary, *in* Mange, M. A., and Wright, D. T., eds., Heavy Minerals in Use: Elsevier, Developments in Sedimentology, v. 58, p.433-436

Mange, M.A., Turner, P., Ince, D., and Wright, D.T., 2007, High-resolution heavy mineral and

Magnetostratigraphy: a powerful tool for subdivision and correlation of barren successions: an example from the Sherwood Sandstone Group (Triassic) of the East Irish Sea Basin and surrounding areas, *in* Mange, M.A., and Wright, D.T., eds., Heavy Minerals in Use: Elsevier, Developments in Sedimentology, v. 58, p. 1073–1097.

Marsaglia, K.M., 1991, Provenance of sands and sandstones from the Gulf of California, a rifted continental arc, *in* Fisher, R.V., and Smith, G.A., eds., Sedimentation in Volcanic Settings: SEPM, Special Publication 45, p. 237–248.

Marsaglia, K.M., 1992, Petrography and provenance of volcaniclastic sands recovered from the Izu–Bonin Arc, Leg 126: Proceedings of the Ocean Drilling Program, Scientific Results, v. 126, p. 139–54.

Marsaglia, K.M., 1993, Basaltic island sand provenance, *in* Johnsson, M.J., and Basu, A., eds., Processes Controlling the Composition of Clastic Sediments: Geological Society of America, Special Paper 284, p. 41–65.

Marsaglia, K.M., and Ingersoll, R.V., 1992, Compositional trends in arc-related, deep-marine sand and sandstone: A reassessment of magmatic-arc: Geological Society of America, Bulletin, v. 104, p. 1637–1649.

Marsaglia, K.M., and Tazaki, K.. 1992, Diagenetic trend in ODP Leg 126 sandstones, *in* Taylor, B., Fujioka, K., et al., eds., Proceedings of the Ocean Drilling Program, Scientific Results: Ocean Drilling Program, College Station, Texas, v. 126, p. 125–138.

Marsaglia, K.M., and Devaney, K., 1995, Tectonic and magmatic controls on backarc basin sedimentation: The Mariana Region re-examined, *in* Taylor, B., ed., Backarc Basins: Tectonics and Magmatism,: Plenum, New York, p. 497-520.

Marsaglia, K.M., Barone, M., Critelli, S., Busby, C., and Fackler-Adams, B., 2016, Petrography of volcaniclastic rocks in intra-arc volcano-bounded to fault-bounded basins of the Rosario segment of the Lower Cretaceous Alisitos oceanic arc, Baja California, Mexico: Sedimentary Geology, v. 336, p. 138–146.

Meinhold, G., 2010, Rutile and its applications in earth sciences: Earth-Science Reviews, v. 102, p. 1-28.

Morris, R.A., DeBari, S.M., Busby, C., Medynski, S., and Jicha, B.R., 2019, Building arc crust: plutonic to volcanic connections in an extensional oceanic arc, the Southern Alisitos Arc, Baja California: Journal of Petrology, v. 60, p. 1195–1228.

Morrone, C., De Rosa, R., Le Pera, E., and Marsaglia, K.M., 2017, Provenance of volcaniclastic beach sand in a magmatic-arc setting: an example from Lipari island (Aeolian archipelago, Tyrrhenian Sea): Geological Magazine, v. 154, p. 804–828.

Morrone, C., Le Pera, E., Marsaglia, K.M., and De Rosa, R., 2020, Compositional and textural study of modern beach sands in the active volcanic area of the Campania region (southern Italy): Sedimentary Geology, v. 396, no. 105567.

Morrone, C., Le Pera, E., Marsaglia, K.M., and De Rosa, R., 2021, Provenance controls on volcaniclastic beach sand: example from the Aeolian archipelago, Mediterranean Sea, *in* Di Capua, A., De Rosa, R., Kereszturi, G., Le Pera, E., Rosi, M. and Watt, S.F.L., eds., Volcanic Processes in the Sedimentary Record: When Volcanoes Meet the Environment: Geological Society of London, Special Publications, 520, http://dx.doi.org/10.1144/SP520-2021-91.

Morton, A.C., 1984, Stability of detrital heavy minerals in Tertiary sandstones of the North Sea Basin: Clay Minerals, v. 19, p. 287–308.

Morton, A.C., and Chenery, S., 2009, Detrital rutile geochemistry and thermometry as guides to provenance of Jurassic-Paleocene sandstones of the Norwegian Sea: Journal of Sedimentary Research, v. 79, p. 540–553.

Morton, A.C., and Hallsworth, C.R., 1999, Processes controlling the composition of heavy mineral assemblages in sandstones: Sedimentary Geology, v. 124, p. 3–29.

Morton, A.C., and Hallsworth, C., 2007, Stability of detrital heavy minerals during burial diagenesis, *in* Mange, M.A., and Wright, D.T., eds., Heavy Minerals in Use: Elsevier, Developments in Sedimentology, v. 58, p. 215–245.

Morton, A.C., and Smale, D., 1990, The effects of transport and weathering on heavy minerals from the Cascade River, New Zealand: Sedimentary Geology, v. 68, p. 117–123.

Naidu, K.B., Reddy, K.S.N., Sekhar, C.R., Rao, P.G., and Krishna, K.N.M., 2020, Rutile mineral chemistry as a guide to provenance of red sediments and modern sands of Bhimunipatnam–Konada Coast, Andhra Pradesh, East Coast of India: National Academy Science (India), Letters, v. 43, p. 145-152.

Palomares, M., and Arribas, J., 1993, Modern stream sands from compound crystalline sources: Composition and sand generation index, *in* Johnsson, M.J., and Basu, A., eds., Processes Controlling the Composition of Clastic Sediments: Geological Society of America, Special Paper 284, p. 313-322.

Palomares, M., Tortosa, A., and Arribas, J., 1989, Estudio de la fracción pesada de arenas actuales derivadas del Sistema Central y su aplicación a los estudios de procedencia: Boletin Geologico y Minero, v. 45, p. 205-213.

Parfenoff, A., Pomerol, C. and Tourenq, J., 1970, Les minéraux en grains. Méthodes d'étude et determination: Masson et Cie., Paris, 578 p.

Peterson, G.L., and Abbott, P.L., 1979, Mid-Eocene climatic change, Southwestern California and Northwestern Baja California: Palaeogeography, Palaeoclimatology, Palaeoecology, v. 26, p. 73-87.

Pettijohn, F.J., 1975, Sedimentary Rocks: Harper and Brothers, New York, 628 p.

Picard, M.D., and McBride, E.F., 1993, Beach sands of Elba Island, Tuscany, Italy: roundness study and evidence of provenance, *in* Johnsson, M.J., and Basu, A., eds., Processes Controlling the Composition of Clastic Sediments: Geological Society of America, Special Paper 284, p. 235–245.

Povondra, P., Lang, M., Pivec, E., and Ulrich, J., 1998, Tourmaline from the Přibyslavice peraluminous alkali-feldspar granite, Czech Republic: Journal of the Czech Geological Society, v. 43, p. 3-8.

Salata, D., 2014, Detrital tourmaline as an indicator of source rock lithology: an example from the Ropianka and Menilite formations (Skole Nappe, Polish Flysch Carpathians): Geological Quarterly, v. 58, p. 19-30.

Servicio Geologico Mexicano, 2000, Carta geologica-minera Lazaro Cardenas(H11-5-6) and PuntaSan Antonio (H11-9) Baja California, (Mexico), scale 1:250000. https://www.sgm.gob.mx/GeoInfoMexGobMx/).

Schmid, R., 1981, Descriptive nomenclature and classification of pyroclastic deposits and fragments of the IUGS Subcommission on the Systematics of Igneous Rocks: Geology, v. 9, p. 41-43.

Shukis, P.S., and Ethridge, F.G., 1975, A petrographic reconnaissance of sand size sediment: upper St. Francis River, southeastern Missouri: Journal of Sedimentary Petrology, v. 45, p. 115-127.

Silver, L.T., and Chappal, B.W., 1988, The Peninsular Ranges batholith: an insight onto the evolution of cordilleran batholiths of southwestern North America: Royal Society of Edinburgh Transactions, Earth Science, v. 79, p. 105–121.

Silver, L.T., Stehli, F.G., and Allen, C.R., 1963, Lower Cretaceous prebatholithic rocks of northern Baja California, Mexico: American Association of Petroleum Geologists, Bulletin, v. 47, p. 2054–2059.

Silver, L.T., Taylor, H.P., and Chappell, B., 1979, Some petrological and geochronological observations of the Peninsular Ranges batholith near the international border of the U.S.A. and Mexico: Geological Society of America, Annual Meeting, Field Trip Guide, Boulder, Colorado, p. 83– 110.

Singh, B.P., Pawar, J.S., and Karlupia, S.K., 2004, Dense mineral data from the northwestern

Himalayan foreland sedimentary rocks and recent river sediments: evaluation of the hinterland: Journal of Asian Earth Sciences, v. 23, p. 25-35.

Smale, D., 2007, Sediment trails in tectonically active islands: heavy minerals in use in New Zealand, *in* Mange, M.A., and Wright, D.T., eds., Heavy Minerals in Use: Elsevier, Developments in Sedimentology, v. 58, p. 569–585.

Smith, G.A., and Lotosky, J.E. 1995, What factors control the composition of andesitic sand?: Journal of Sedimentary Research, v. A65, p.91–98.

Suttner, L.J., 1974, Sedimentary petrographic provinces: an evaluation, *in* Ross C.A., ed., Paleogeographic Provinces and Provinciality: SEPM, Special Publication, 21, p. 75–84.

Tangari, A.C., Scarciglia, F., Piluso, E., Marinangeli, L., and Pompilio, L., 2018, Role of weathering of pillow basalt, pyroclastic input and geomorphic processes on the genesis of the Monte Cerviero upland soils (Calabria, Italy): Catena, v. 171, p. 299-315.

Tangari, A.C., Le Pera, E., Andò, S., Garzanti, E., Piluso, E., Marinangeli, L., and Scarciglia, F., 2021, Soil-formation in the central Mediterranean: insight from heavy minerals: Catena, v. 197, no.104998.

Turner, G., and Morton, A.C., 2007, The effects of burial diagenesis on detrital heavy mineral grain surface textures, *in* Mange, M.A., and Wright, D.T. eds., Heavy Minerals In Use: Elsevier, Developments in Sedimentology, v. 58, p. 393–412

Van Loon, A.J., and Mange, A.M., 2007, "In situ" dissolution of heavy minerals through extreme weathering, and the application of the surviving assemblages and their dissolution characteristics to correlation of Dutch and German silver sands, *in* Mange, M.A., and Wright, D.T., eds., Heavy Minerals in Use: Elsevier, Developments in Sedimentology, v. 58, p. 189–213.

Velbel, M.A., 2007, Surface textures and dissolution processes of heavy minerals in the sedimentary cycle: examples from pyroxenes and amphiboles, *in* Mange, M.A., and Wright, D.T., eds., Heavy Minerals in Use: Elsevier, Developments in Sedimentology, v. 58, p. 113- 150.

Velbel, M.A., Basso, C.L., and Zieg, M.J., 1996, The natural weathering of staurolite: crystal surface textures, relative stability, and the rate-determining step: American Journal of Science, v. 296, p. 453-472.

Vezzoli, G., Garzanti, E. and Monguzzi, S., 2004, Erosion in the Western Alps (Dora Baltea basin) 1. Quantifying sediment provenance, *In* Weltje, G.J. and von Eynatten, H., eds., Quantitative Provenance Analysis of Sediments: Sedimentary Geology, v. 171, p. 227–246.

Yücel-Öztürk, Y., Helvac, C., Palmer, M.R., Ersoy, E.Y., and Freslon, N., 2015, Origin and significance of tourmalinites and tourmaline-bearing rocks of Menderes Massif, western Anatolia, Turkey: Lithos, v. 218-219, p. 22-36.

Walawander, M.J., Gastil, R.G., Clinkenbeard, J.P., McCormick, W.V., Eastman, B.G., Wenicke, R.S., Wardlaw, M.S., Gunn, S.H., and Smith, B.M., 1990, Origin and evolution of the zoned La Posta-type plutons, eastern Peninsular Ranges batholith, southern and Baja California, *in* Anderson, J.L., ed., The Nature and Origin of Cordilleran Magmatism: Geological Society of America, (Boulder, CO) 174 p. 1– 18.

Weltjie, GJ., 1992, Oligocene to Early Miocene sedimentation and tectonics in the southern part of the Calabrian-Peloritan Arc (Aspromonte, southern Italy): a record of mixed-mode piggy-back basin evolution: Basin Research, v. 4, p. 37-68.

White, N., Pringle, M., Garzanti, E., Bickle, M., Najman, Y., Chapman, H., and Friend, P., 2002, Constraints on the exhumation and erosion of the High Himalayan slab, NW India, from foreland basin deposits: Earth Planetary and Science Letters, v. 195, p. 29–44.

Wilson, F.A.,1981, Preliminary investigations of accessory zircon from volcanic and sedimentary rocks from Clear Lake: USGS (United States Geological Survey), Professional Paper 1141, p. 251-259.

Wotzlaw, J.F., Decou, A., von Eynatten, H., Worner, G., and Frei, D., 2011, Jurassic to Palaeogene tectono-magmatic evolution of northern Chile and adjacent Bolivia from detrital zircon U-Pb geochronology and heavy mineral provenance: Terra Nova, v. 23, p. 399-406.

Zoleikhaei, Y, Mulder, J.A., and Cawood, P.A.,2021, Integrated detrital rutile and zircon provenance reveals multiple sources for Cambrian sandstones in North Gondwana: Earth-Science Reviews, v.213, p.1-29.

Zuffa, G.G., 1980, Hybrid arenites: their composition and classification: Journal of Sedimentary Petrology, v. 50, p. 21–29.

Zuffa, G.G., 1985, Optical analyses of arenites: Influence of methodology on compositional results, *in* Zuffa, G.G., ed., Provenance of Arenites: Dordrecht, Netherlands, D. Reidel, NATO Advanced Study Institute Series, v. 148, p. 165–189

Zuffa, G.G., 1987, Unravelling hinterland and offshore paleogeography from deep-water arenites, *in* Leggett, J.K. and Zuffa, G.G., eds. Marine Clastic Sedimentology: Graham and Trotman, London, p. 39-61.

## FIGURE CAPTIONS

Fig. 1. — Geological map of the study area (modified from Servicio Geologico Mexicano https://www.sgm.gob.mx/GeoInfoMexGobMx/) with the location of sampling sites.

Fig. 2. — Ternary compositional diagrams. **A)** Framework petrography (Q, quarz; F, feldspar; L, lithic fragments) (e.g., Garzanti, 2016, 2019). **B)** Qm, monocrystalline quartz; K, potassium feldspar;

Pl plagioclase. **C)** Lithic fragments (Lm, metamorphic; Lv, volcanic; Ls, sedimentary) (e.g., Ingersoll and Suczek, 1979). **D)** Qp, policrystalline quartz; Lvm, volcanic and metavolcanic lithic fragments; Lsm, sedimentary and metasedimentary lithic fragments. **E)** Rg, granitic/gneissic rock fragments, Rv, volcanic rock fragments, Rm, metamorphic rock fragments (e.g., Critelli and Le Pera, 1994; Critelli and Ingersoll, 1995).

Fig. 3.— Ternary compositional diagrams of lithic fragments. **A)** Ls, sedimentary; Lm1, low-grade metamorphic; Lm2, medium-grade metamorphic (e.g., Dorsey 1988). **B)** Proportions of volcanic rock-fragment textures (Lvf, felsitic texture; Lvmi, microlitic; Lvl, lathwork) (e.g., Marsaglia 1993; Critelli et al. 2002; Morrone et al. 2017, 2020). **C)** Comparison between the relative proportions of Lvf, Lvmi, and Lvl in the river sand analyzed in this study (green circle, San Fernando River; red circle, San Vicente River; blue circle, El Rosario River) to other volcanic settings.

Fig. 4.— Photomicrographs from petrographic thin sections illustrating diagnostic grains of El Rosario (A-D), San Fernando (E, F), and San Vicente (G, H) rivers. **A, B**) Monocrystalline grains of quartz (Qz), plagioclase (Pl), biotite (Bt) and hornblende (Hbl), polymineralic grains made up of quartz, biotite and feldspar (Qz in Rg). **C, D)** Monomineralic grains of altered (Pl alt) and zoned plagioclase (Pl), quartz grains (Qz). **E)** Quartz overgrowth on a monomineralic grain. **F)** Carbonate cement surrounding a quartz grain. **G, H)** Opaque mineral in a volcanic lithic with lathwork texture (Op in Lvl), quartz phenocryst in a volcanic lithic with felsitic seriate texture (Qz in Lvf), epidotized plagioclase (Plalt), Epidote (Ep). A, C, E, F, and G are crossed-nicols photomicrographs, and B, D, and H are plane-polarized-light photomicrographs. A-D are from sample SC251. E, F are from sample SC217. G, H are from sample SC237.

Fig. 5. —Photomicrographs from petrographic thin sections illustrating diagnostic grains of San Fernando (A-D; G, H) and El Rosario (E, F) rivers. **A, B)** Volcanic lithic with lathwork texture (Lvl)

with black (upper) and orange (lower) glassy groundmass, pyroxene phenocrysts immersed in a black and orange glassy groundmass (Px), plagioclase phenocryst immersed in a black glassy groundmass and plagioclase single crystal grains (Pl, lower right), volcanic lithic with microlitic texture with brown glassy groundmass (Lvmi). **C, D)** Volcanic lithic with lathwork texture (Lvl) made up of laths of plagioclase (Pl) and pyroxene (upper Px) immersed in a brown and black glassy groundmass, pyroxene single crystal (Px), quartz single crystal (Qz), siltstone with micritic matrix (Ss), granitoid rock fragment (Rg), volcanic lithic with microlitic texture; microlites are immersed in a brown glassy groundmass (Lvmi). **E, F)** Volcanic lithic with holocrystalline texture (Lvo) (Marsaglia 1993) with hornblende and biotite. **G, H)** Volcanic lithic with vitric texture (Lvv), volcanic lithic with lathwork texture (Lvl) with pyroxene (Px) phenocrysts immersed in a brown glassy groundmass, calcite single spar (Cal), monocrystalline quartz (Qz), polycrystalline quartz (Qp), plagioclase single crystals (Pl). A, C, E, and G are crossed-nicols photomicrographs, and B, D, F, and H are plane-polarized-light photomicrographs. A and B are from SC215. C and D are from sample SC210. E, F are from sample SC262 sample and G, H are from sample SC209.

Fig. 6. — Photomicrographs from petrographic thin sections illustrating diagnostic grains of San Fernando rivers (A-H). **A, B)** Tourmaline (Tur), plagioclase (Pl), and quartz (Qz) single crystals, polymineralic volcanic (Lvmi) and sedimentary (SS = sandstone) lithic grains, volcanic lithic in sandstone grain (Lv in SS). **C)** Metamorphic (Lm) and sedimentary (Ss = siltstone) lithic grains, volcanic lithics with plagioclase phenocrysts (Lvl), altered and undetermined volcanic lithic fragment (Lvalt), polycrystalline (Qp) and monocrystalline (Qz) quartz grains, plagioclase single crystal (Pl). **D)** Volcanic lithic fragment with microlitic texture (Lvmi), silt-size sedimentary lithic fragment (Ss = siltstone), polycrystalline quartz (Qp), and plagioclase single crystal (Pl). **E, F)** Volcanic lithics with lathwork (Lvl), microlitic (Lvmi), and felsitic (Lvf) texture, altered and undetermined volcanic lithic fragment (Lvalt), metamorphic lithic fragment (Lm) quartz (Qz), plagioclase (Pl) and hornblende (Hbl) single crystals. **G)** Zoned plagioclase (Pl) and hornblende (Hbl) in a granitoid rock

fragment (Rg), plagioclase single crystal (Pl). **H)** Quartz (Qz), plagioclase (Pl), and hornblende (Hbl) in a granitoid rock fragment (Rg), pyroxene single crystal (Px). A, C, D, E, G, and H are crossed-nicols photomicrographs, and B and F are plane-polarized-light photomicrographs. A, B, E, and F are from sample SC215. C and D are from sample SC213. G is from sample SC217 and H is from sample SC212.

Fig.7. — Photomicrographs from petrographic thin sections illustrating diagnostic grains of San Vicente (A-D) and San Fernando (E-H) rivers. **A, B)** Rounded volcanic lithic grains with microlitic texture (Lvmi), altered plagioclase with sericite and clay minerals replacement (Plalt), volcanic lithic with felsitic granular texture (Lvf), granitoid rock fragment (Rg). **C, D)** Vesiculated volcanic lithic grain with microlitic texture and black glass (Lvmi), metasedimentary lithic fragment (Lsm), plagioclase single crystal (Pl), metamorphic lithic fragment (Lm), K-feldspar single crystal (K). **E, F)** Altered and undetermined volcanic lithic fragment showing vesicles replaced with chlorite and clays (Lvalt), plagioclase in a granitoid rock fragment (Pl in Rg), polymineralic grains made up of quartz, biotite, and feldspar (Rg), bended biotite flake (Bt), volcanic lithic fragments with plagioclase laths (Lvl) and microlites (Lvmi), plagioclase single crystal (Pl). **G, H)** Hyaloclastite grain with vesicles filled by zeolite (**Zeo**) and clay minerals and with palagonite and zeolite replacement of original glass (**Pal**). A, C, E, and G are crossed-nicols photomicrographs, and B, D, F, and H are plane-polarized-light photomicrographs. A is from sample SC236. C and D are from sample SC229. E and H are from sample SC215.

Fig.8. — Histograms showing the abundance of the detrital modes from the upstream to the downstream in all three river systems. **A)** Quartz (Q), Feldspar(F), and lithic fragment (Lt) abundance. **B)** Lithic fragments abundance: Lm = metamorphic lithic fragments, Lv = volcanic lithic fragments, Ls = sedimentary lithic fragments. **C)** Abundance of various volcanic lithic fragments: Lvf = felsitic texture, Lvmi = microlitic, Lvl lathwork.

Fig.9. — Dissolution of transparent heavy minerals with related surface texture in the river sands of San Fernando (SF), San Vicente (SV), and El Rosario (ER). **A)** Unstable heavy minerals. **A1)** Corroded brown hornblende (SF, SC217) (Hbl), **A2)** etched green-brown hornblende (SF, SC210) (Hbl), **A3)** blueish-green hornblende (SF SC215) (Hbl), **A4)** euhedral (SF, SC218) (Hyp), and **A5)** etched (ER, SC261) (Hyp) hypersthene respectively with spinel inclusions, **A6)** etched diopside (SF, SC211) (Di). **B)** Moderately stable heavy minerals. **B1)** Corroded green epidote (SF SC211) (Ep), **B2)** corroded kyanite (Ky), and **B3)** staurolite with the presence of mamillae on its surface (St) in the SF SC215 respectively, **B4)** corroded colorless garnet (SF SC211) (Grt), **B5)** unweathered titanite (SF SC215) (Tnt), **B6)** corroded colorless titanite (SV SC35) (Tnt). **C)** Stable heavy minerals. **C1)** Euhedral (Zrn) and **C2)** subrounded zircon (Zrn) respectively in the SF SC211, **C3)** subrounded brown tourmaline (SF SC215) (Tur), **C4)** subrounded bluish tourmaline (SF SC217) (Tur), **C5)** subrounded red rutile (SF SC210) (Rt), **C6)** corroded brown rutile (ER SC251) (Rt).

Fig. 10. — **A)** Ternary diagram showing the different provenance of heavy mineral grains. Sedimentary = Zr+Tur+Rt, magmatic = Hbl (oxyhornblende and green-brown in colour) +Cpx+Opx+Ttn), metamorphic = Hbl (blue-green) +Act+Grt+Sill+Ky+And+Ep). **B)** Histogram showing the provenance of the different grains of hornblende. Hbl volcanic = Oxyhornblende+green-brown, Hbl metamorphic = blue-green hornblende. **C)** Ternaryplot exhibiting the main weathering stages of the pyroxene grain. **D)** Ternary plot exhibiting the main weathering stages of the hornblende grains.

Fig.11. — Pie diagrams indicating the distribution of the transparent heavy-minerals grains in the various electromagnetic Frantz fractions expressed in Amperes (Å). ZTR = zircon, tourmaline, and rutile, Ttn = titanite, Ap = Apatite, Amp =Amphibole, Cpx =clinopyroxene, Opx = Orthopyroxene, Ep = Epidote, Grt = Garnet, SKA = Sillimanite, Kyanite, Andalusite.

Fig.12 — Proportion of source rocks in each drainage basin.

## TABLE CAPTIONS

Tab.1. — Grain point counting of light minerals expressed in wt%.

Tab.2. — Heavy-mineral concentrations in the studied river sand samples. Total (HMC) and transparent heavy minerals (tHMC) are expressed as wt%. HCl = hornblende color index; ZTR = zircon, tourmaline, and rutile.

Figure Click here to access/download;Figure;Fig.1.jpg

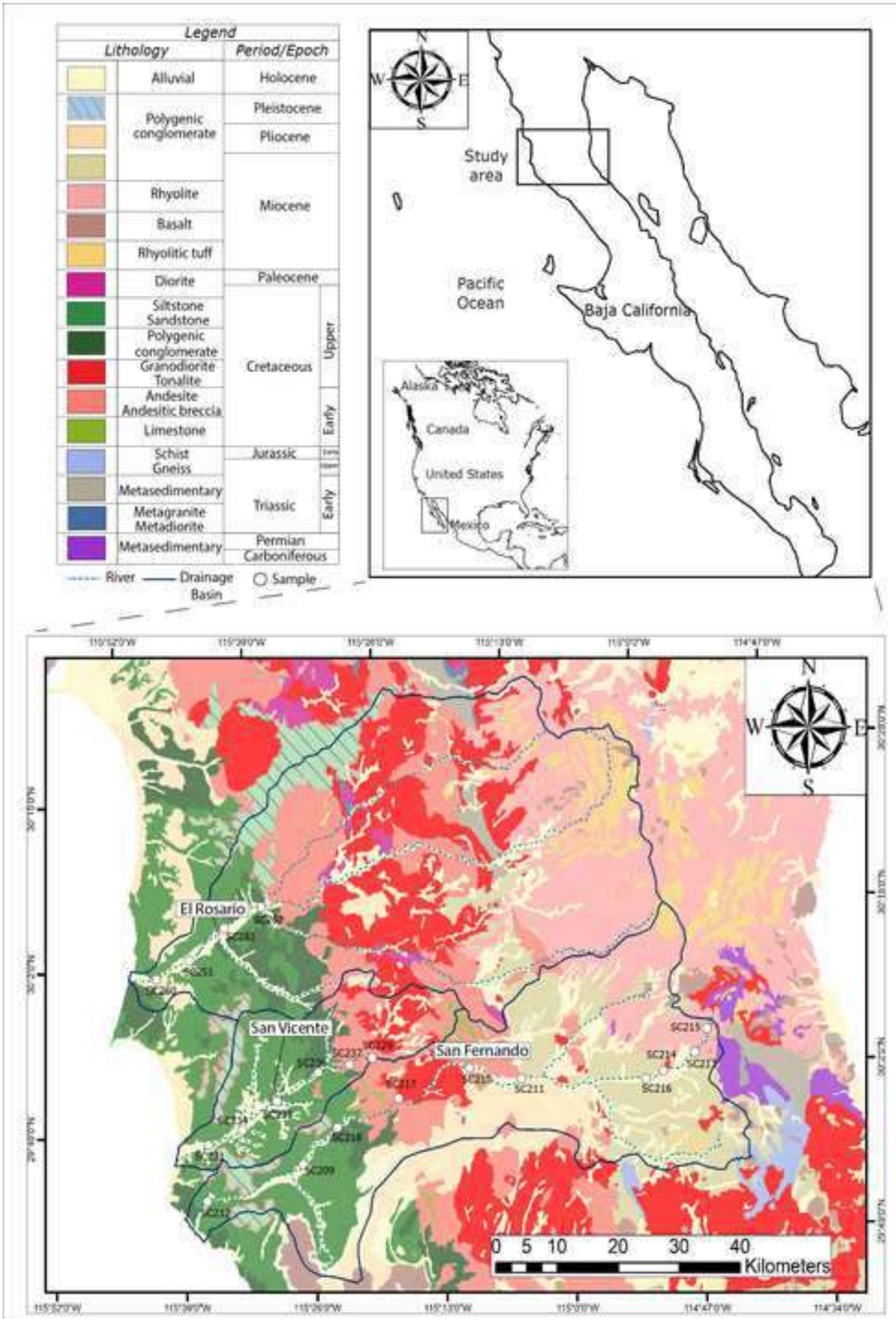

Figure

Click here to access/download;Figure;Fig.2.jpg

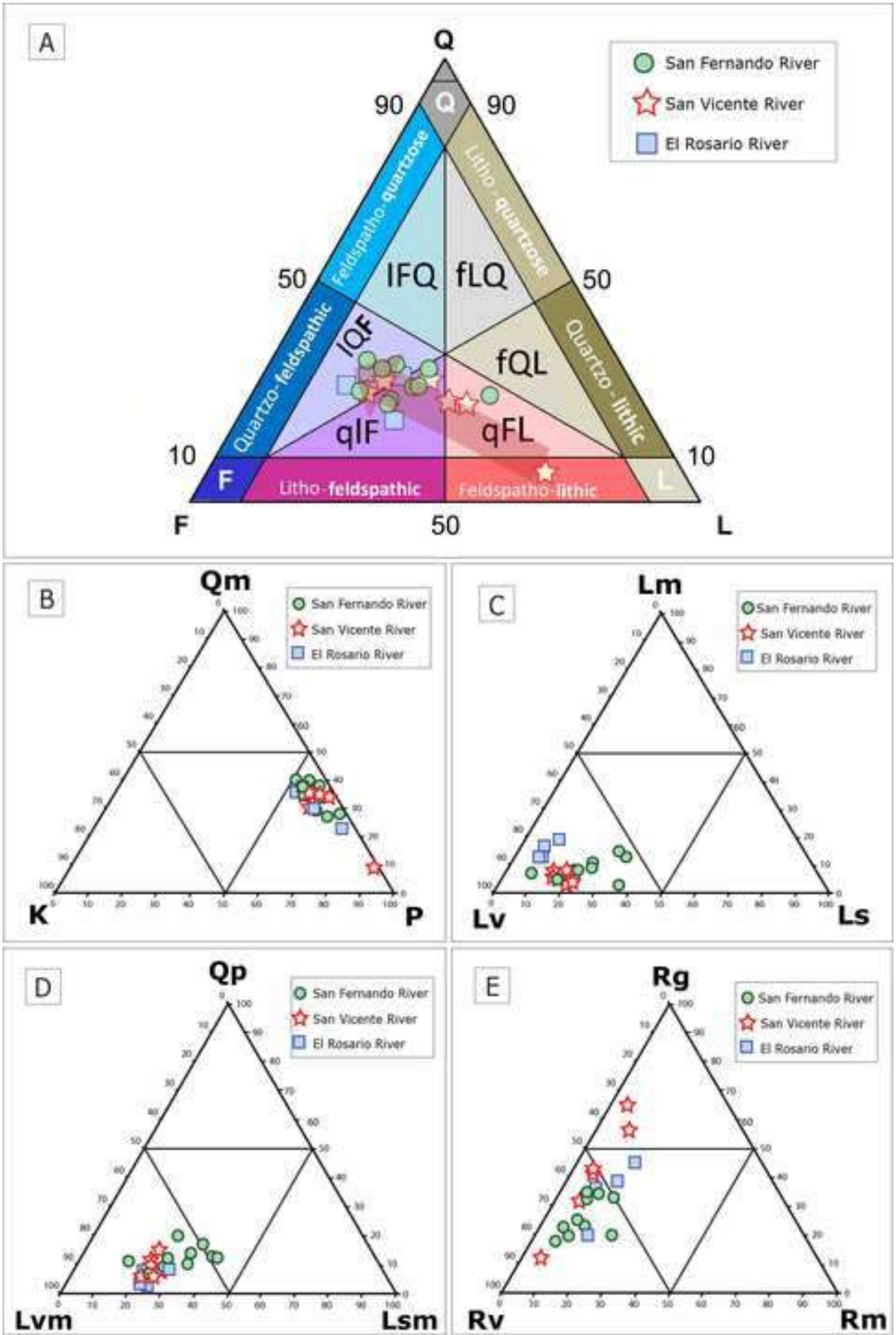

Figure

Click here to access/download;Figure;Fig.3.jpg

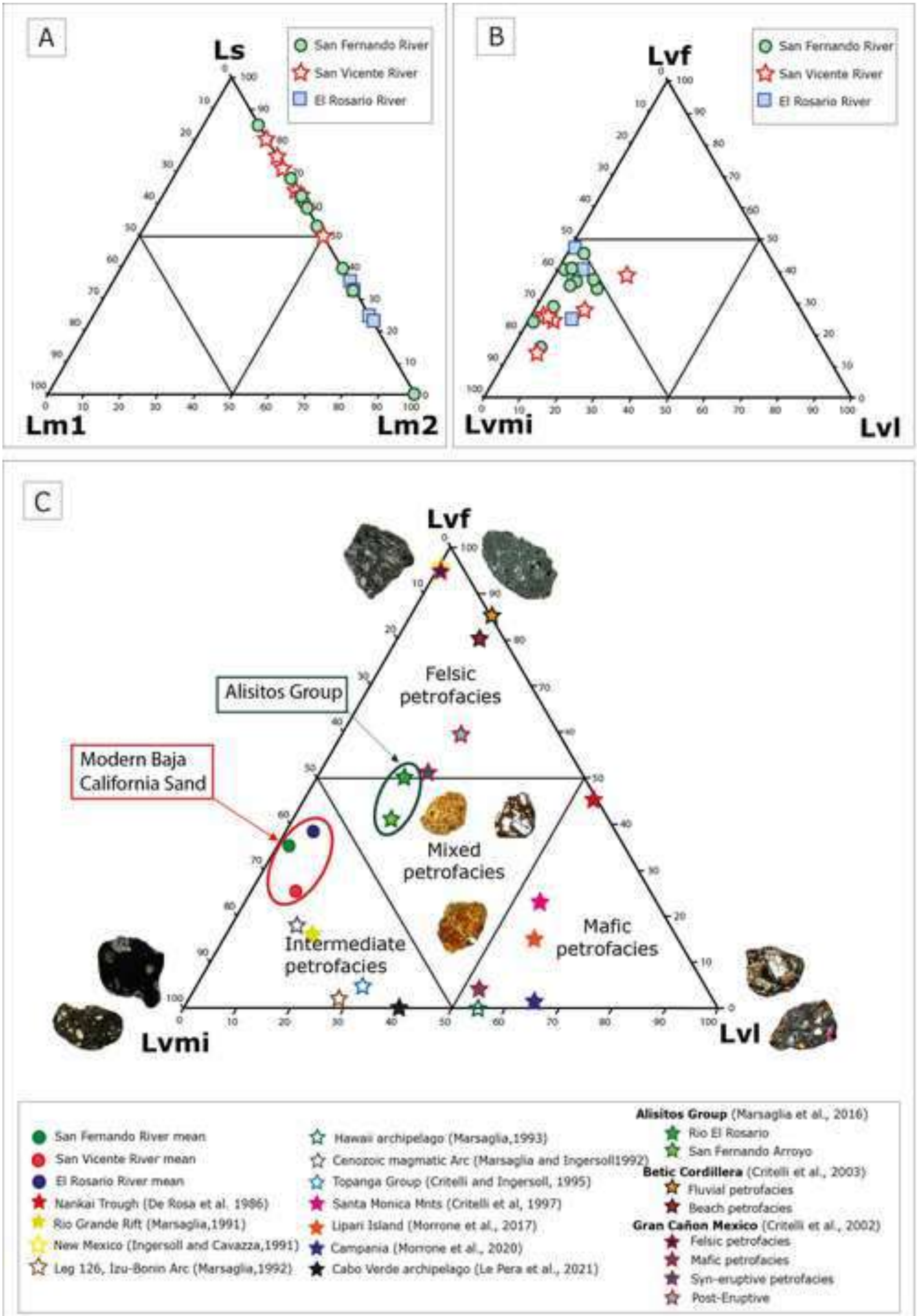

Figure

Click here to access/download;Figure;Fig.4.jpg

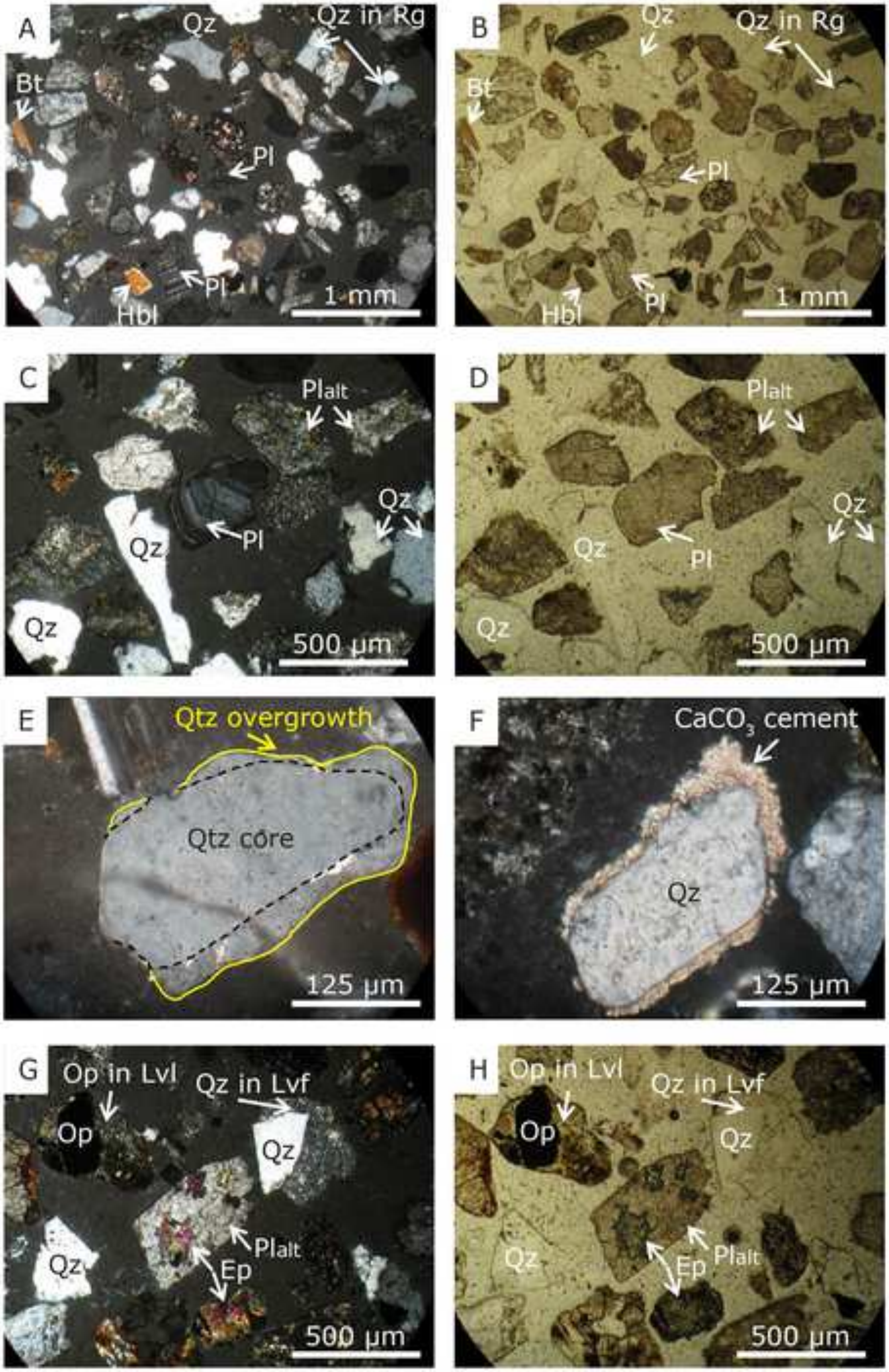

Figure



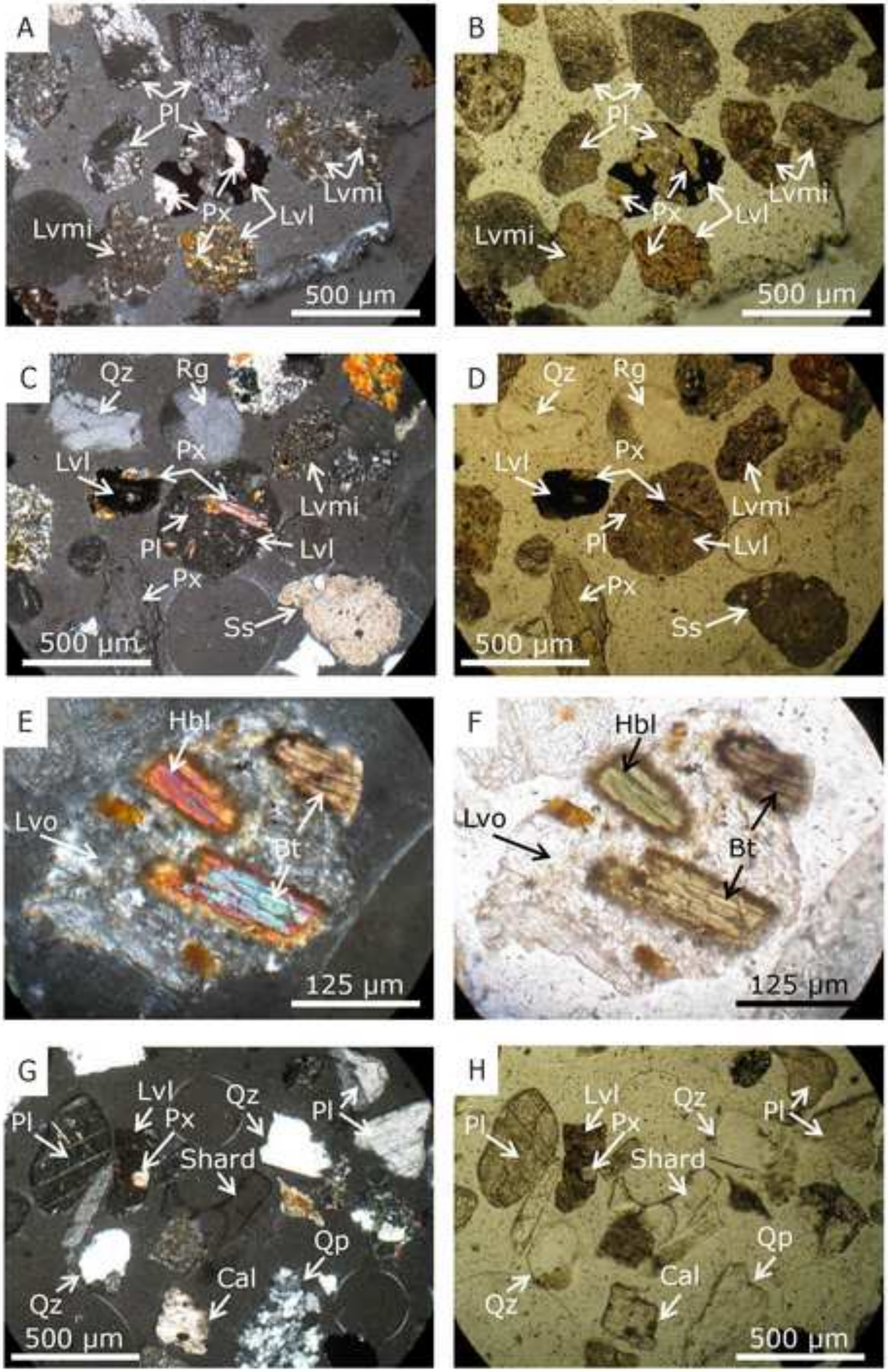

A
Pl
Lvmi
Px
Lvl
Lvmi
500 µm
B
Pl
Lvmi
Px
Lvl
Lvmi
500 µm
C
Qz
Rg
Px
Lvl
Lvmi
Pl
Lvl
Px
Ss
500 µm
D
Qz
Rg
Px
Lvl
Lvmi
Pl
Lvl
Px
Ss
500 µm
E
Hbl
Lvo
Bt
125 µm
F
Hbl
Lvo
Bt
125 µm
G
Lvl
Qz
Pl
Pl
Px
Shard
Qp
Cal
Qz
500 µm
H
Lvl
Qz
Pl
Pl
Px
Shard
Qp
Cal
Qz
500 µm

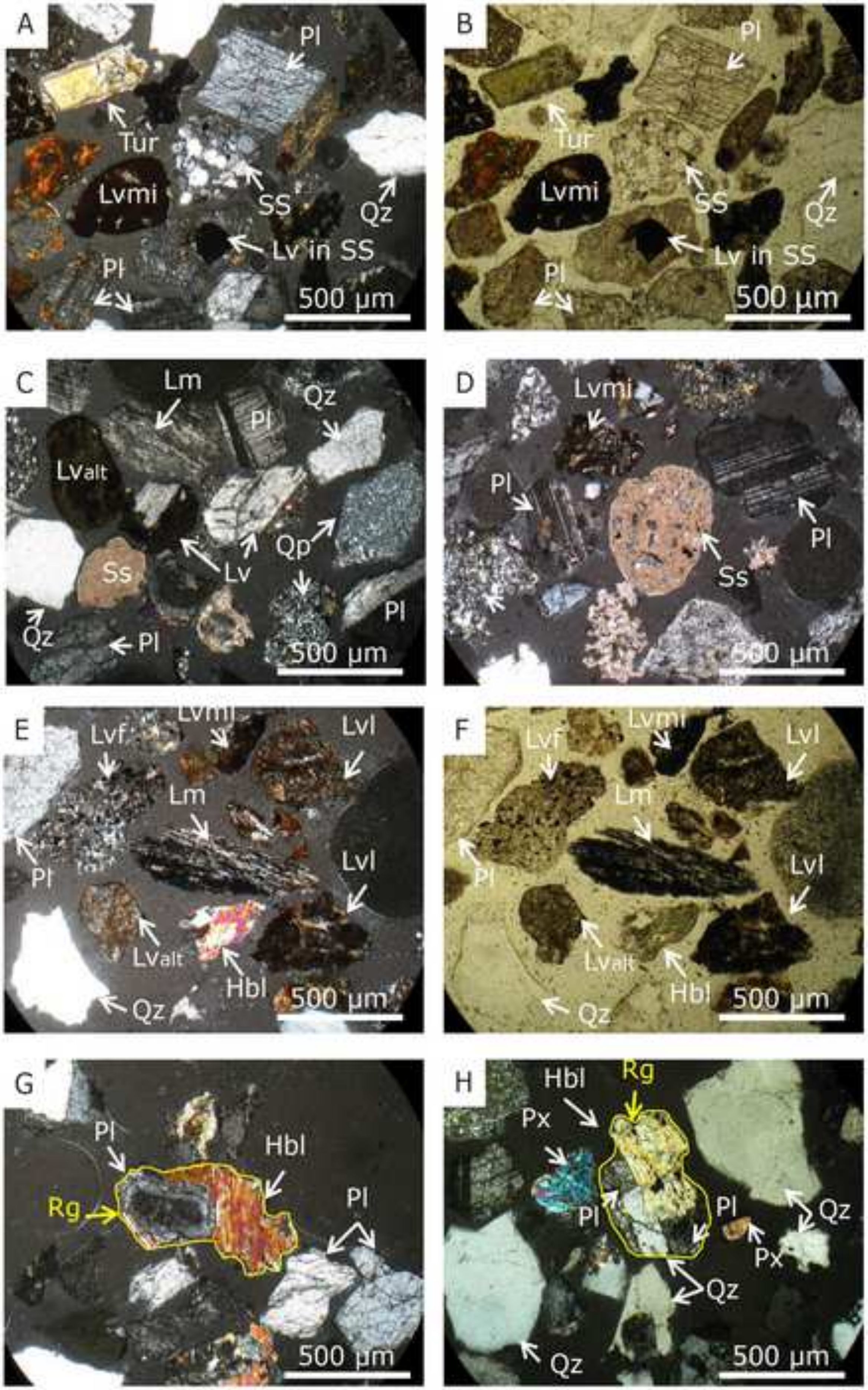
A
Pl
Tur
Lvmi
SS
Qz
Lv in SS
Pl
500 µm
B
Pl
Tur
Lvmi
SS
Qz
Lv in SS
Pl
500 µm
C
Lm
Pl
Qz
Lvalt
Ss
Lv
Qp
Qz
Pl
Pl
500 µm
D
Lvmi
Pl
Pl
Ss
500 µm
E
Lvf
Lvmi
Lvl
Lm
Pl
Lvl
Lvalt
Hbl
Qz
500 µm
F
Lvf
Lvmi
Lvl
Lm
Pl
Lvl
Lvalt
Hbl
Qz
500 µm
G
Pl
Hbl
Rg
Pl
500 µm
H
Hbl
Rg
Px
Pl
Pl
Qz
Px
Qz
Qz
500 µm

Figure

Click here to access/download;Figure;Fig.7.jpg

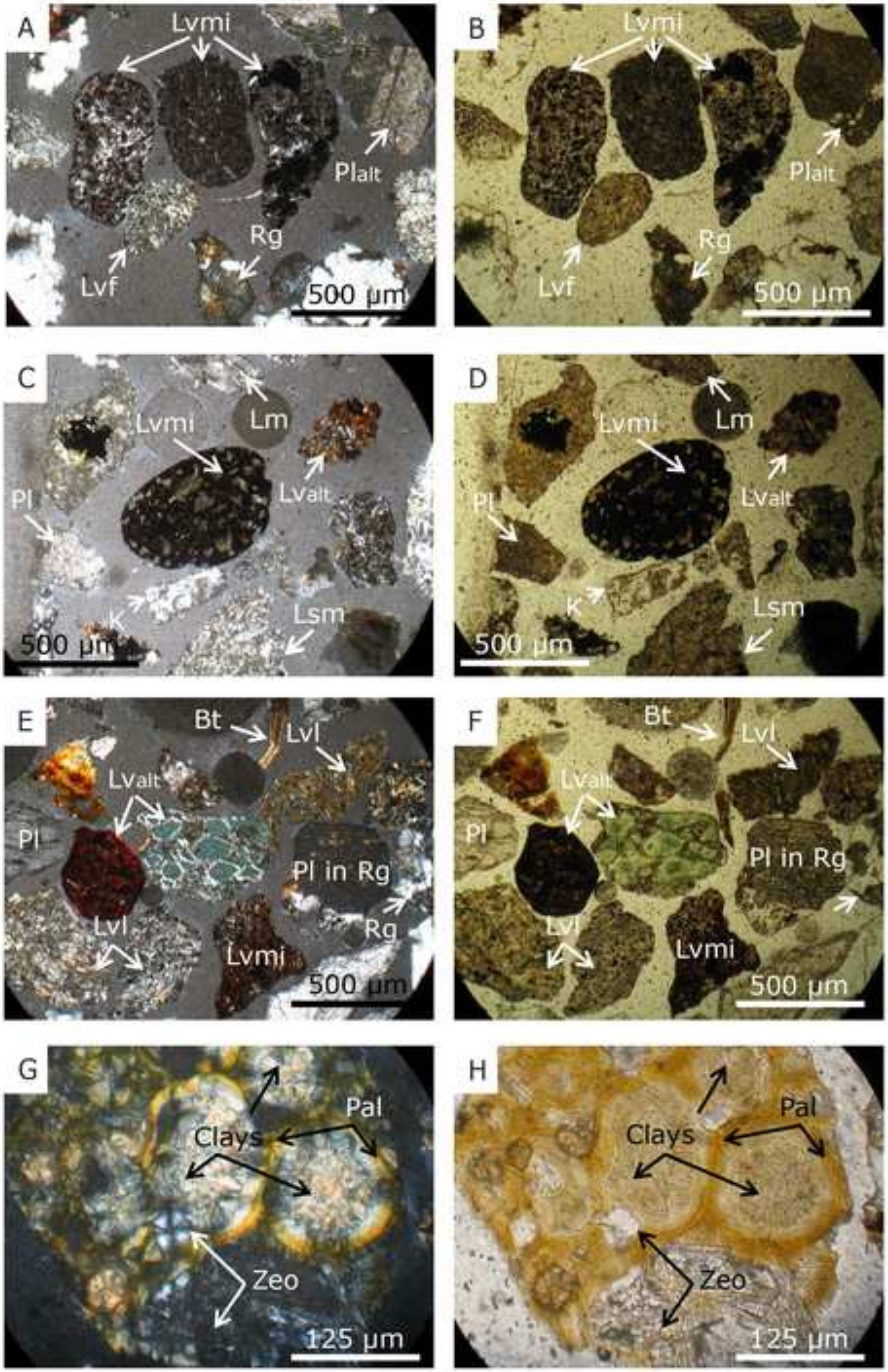

Figure

Click here to access/download;Figure;Fig.8.jpg

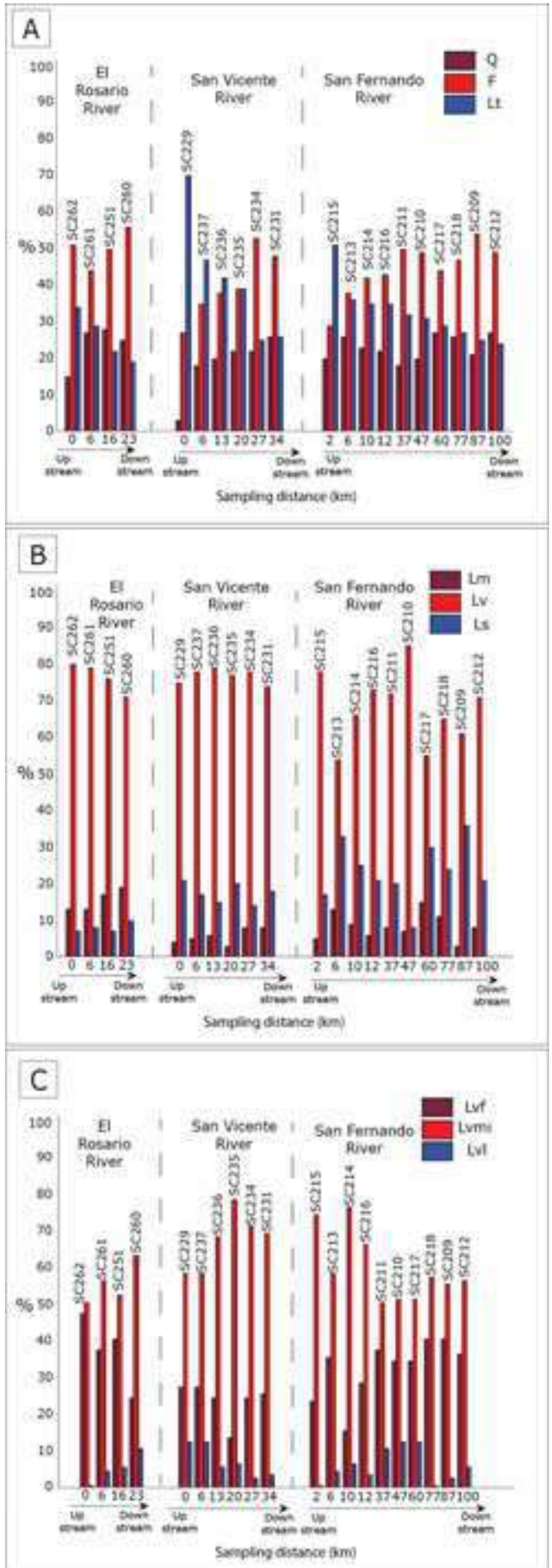

 

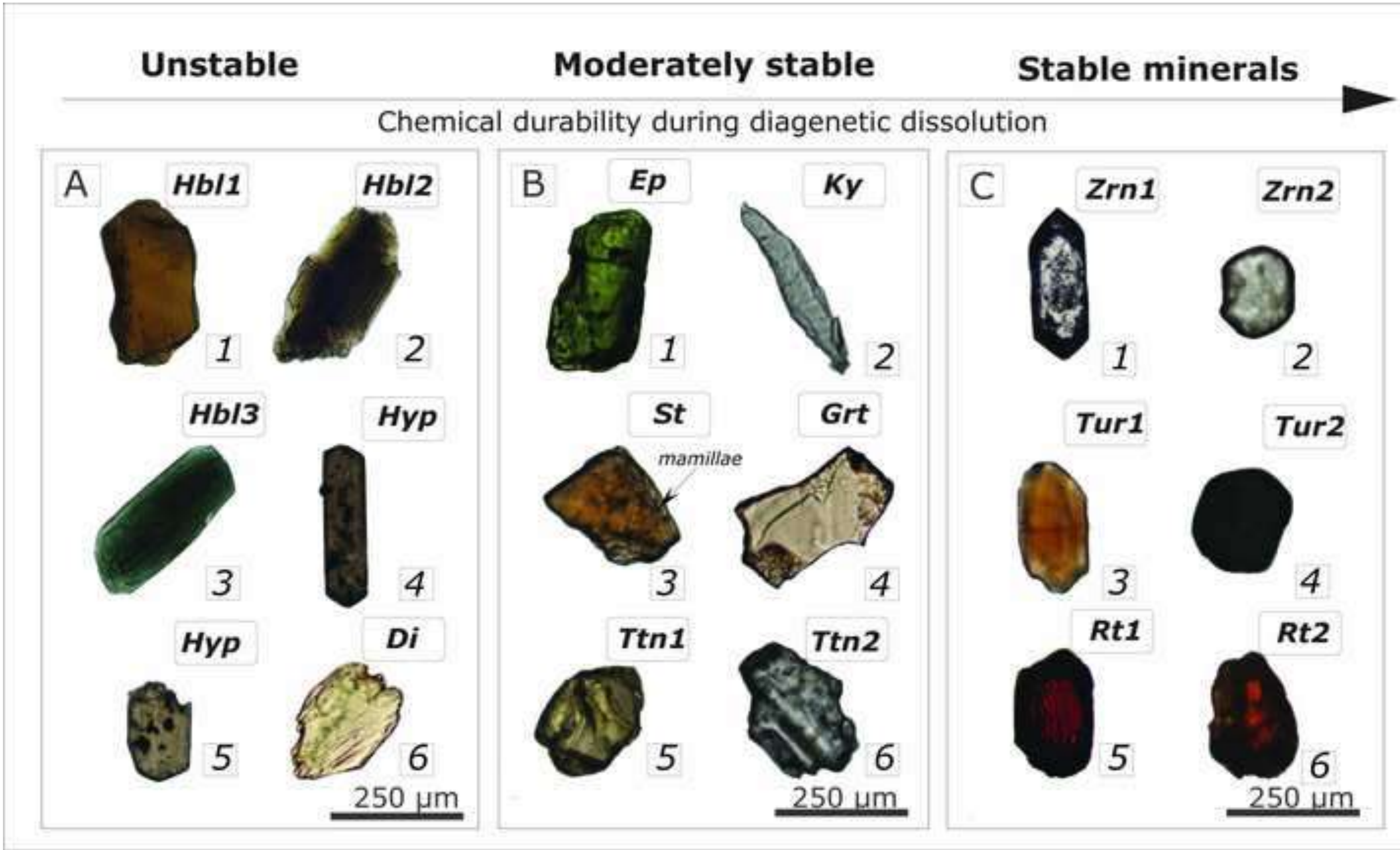
Unstable
Moderately stable
Stable minerals
Chemical durability during diagenetic dissolution
A
Hbl1
Hbl2
1
2
Hbl3
Hyp
3
4
Hyp
Di
5
6
250 μm
B
Ep
Ky
1
2
St
Grt
mamillae
3
4
Ttn1
Ttn2
5
6
250 μm
C
Zrn1
Zrn2
1
2
Tur1
Tur2
3
4
Rt1
Rt2
5
6
250 μm

Figure

Click here to access/download;Figure;Fig.10.jpg

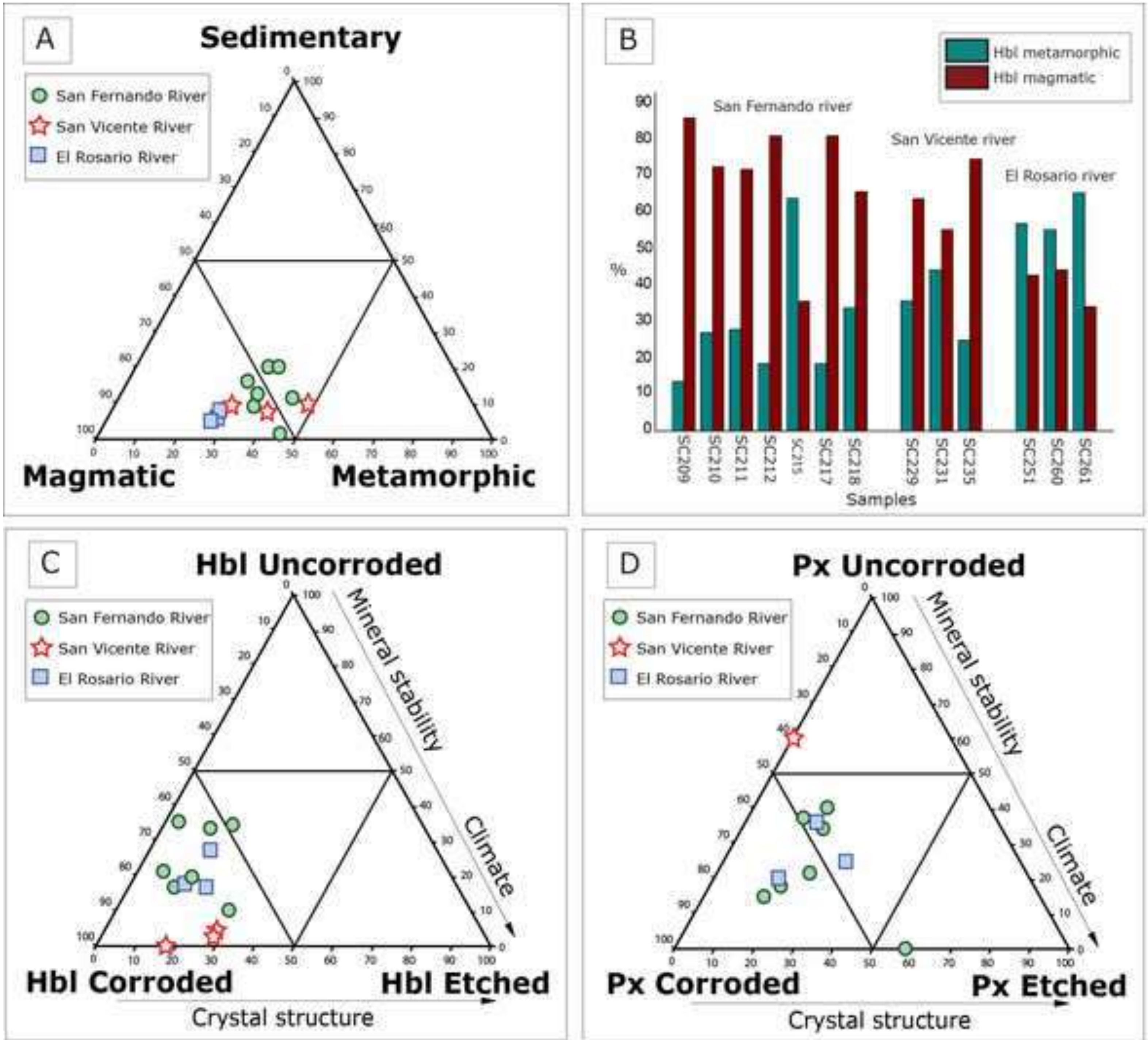

 

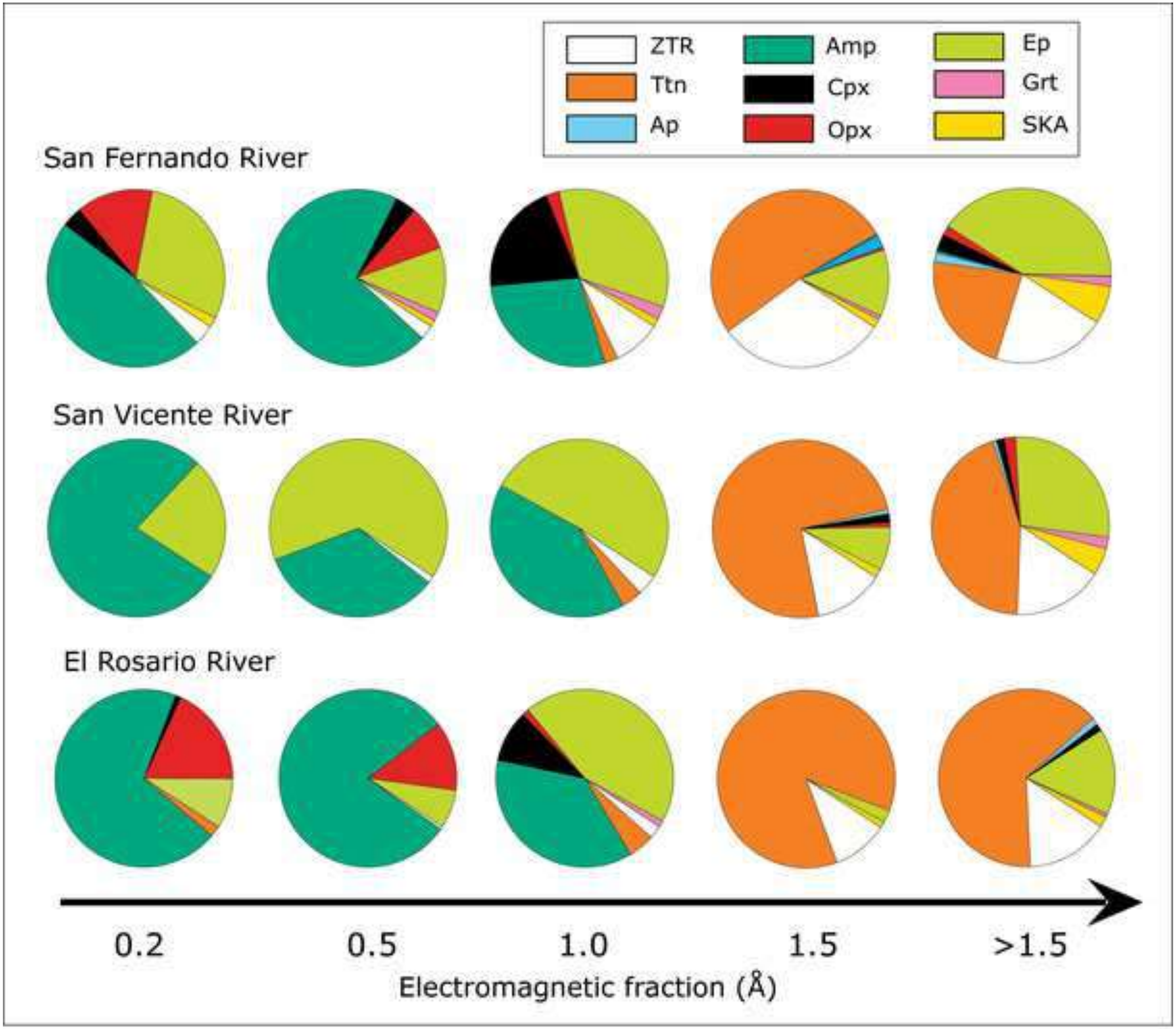
ZTR
Ttn
Ap
Amp
Cpx
Opx
Ep
Grt
SKA
San Fernando River
San Vicente River
El Rosario River
0.2
0.5
1.0
1.5
>1.5
Electromagnetic fraction (Å)

Figure

Click here to access/download;Figure;Fig.12.jpg

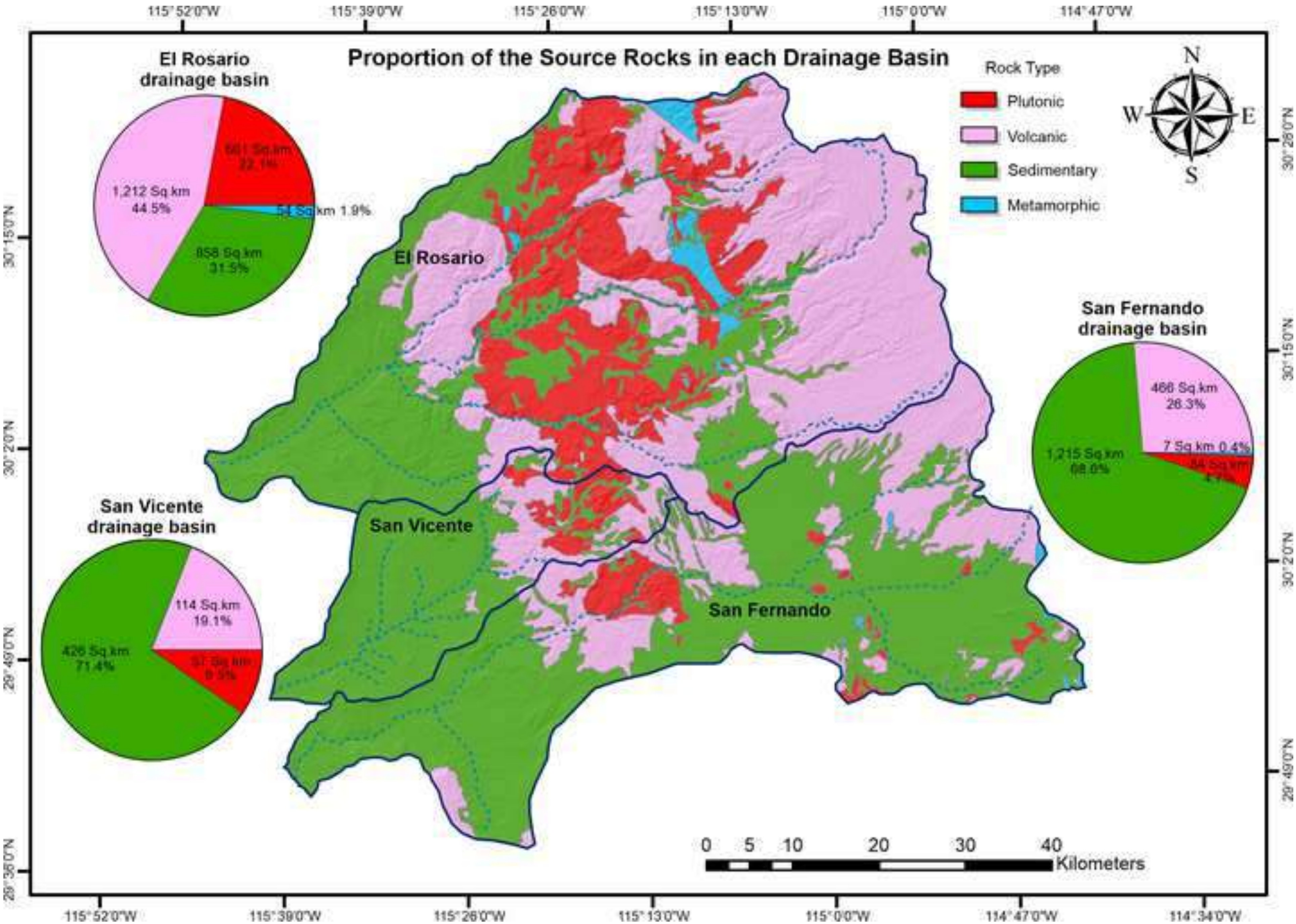

Table

Click here to access/download;Table;Table_1.xlsx

| River | Sample | Q (single crystal) | Qp with tectonic fabric | Qp without tectonic fabric | Q in VRF | Q in MRF | Q in PRF | Q in sandstone | K (single crystal) | K in VRF | K in MRF | K in PRF | K in sandstone | P (single crystal) | P in VRF | P in MRF | P in PRF | P in sandstone | Micas and chlorite (single crystal) | Micas and chlorite in MRF | Micas and chlorite in PRF | Volcanic lithic with microlitic texture | Volcanic lithic with lathwork texture | Volcanic lithic with vitric texture | Volcanic lithic with felsitic granular texture | Volcanic lithic with felsitic seriate texture | Pumice | Volcanic lithic with lathwork texture in sandstone | Subvolcanic-hypabissal lithic | Phyllite | Fine-grained schist | Siltstone | Shale | Volcaniclastic shale | Metavolcanic lithic | Cement or matrix in sandstone | Tourmaline (single crystal) | Epidote (single crystal) | Epidote in VRF | Epidote in PRF | Epidote in MRF | Hornblende (single crystal) | Hornblende in PRF | Hornblende in MRF | Hornblende in VRF | Titanite (single crystal) | Titanite in PRF | Garnet (single crystal) | Opaque (single crystal) | Opaque in PRF | Cordierite (single crystal) | Pyroxene (single crystal) | Pyroxene in VRF | Zircon | Calcite (single spar) | Micritic limestone | Biomicritic limestone | Sparitic limestone | Silty-arenitic limestone | Fe-Oxid concrections | Alterite | Und | Tot | Light minerals % | Heavy minerals % |
|---|---|---|---|---|---|---|---|---|---|---|---|---|---|---|---|---|---|---|---|---|---|---|---|---|---|---|---|---|---|---|---|---|---|---|---|---|---|---|---|---|---|---|---|---|---|---|---|---|---|---|---|---|---|---|---|---|---|---|---|---|---|---|---|---|---|
| San Fernando river | **SC209** | 54 | 0 | 12 | 0 | 1 | 2 | 2 | 3 | 0 | 0 | 2 | 0 | 132 | 4 | 1 | 8 | 1 | 0 | 0 | 0 | 10 | 4 | 4 | 11 | 6 | 0 | 0 | 0 | 1 | 1 | 7 | 4 | 0 | 0 | 0 | 0 | 3 | 0 | 0 | 0 | 10 | 1 | 0 | 1 | 0 | 0 | 0 | 5 | 0 | 0 | 0 | 0 | 0 | 4 | 4 | 0 | 2 | 0 | 0 | 0 | 0 | **300** | 93 | 7 |
| | **SC210** | 44 | 3 | 6 | 0 | 4 | 5 | 1 | 9 | 0 | 0 | 5 | 0 | 104 | 3 | 1 | 10 | 0 | 0 | 0 | 0 | 21 | 15 | 5 | 10 | 10 | 0 | 1 | 4 | 5 | 0 | 0 | 0 | 0 | 0 | 0 | 0 | 5 | 0 | 0 | 0 | 11 | 0 | 0 | 2 | 2 | 0 | 1 | 1 | 6 | 0 | 1 | 1 | 0 | 0 | 3 | 0 | 1 | 0 | 0 | 0 | 0 | **300** | 90 | 10 |
| | **SC211** | 43 | 1 | 9 | 0 | 4 | 3 | 0 | 9 | 0 | 0 | 2 | 0 | 110 | 3 | 0 | 14 | 0 | 3 | 0 | 1 | 30 | 6 | 1 | 10 | 4 | 0 | 0 | 4 | 6 | 0 | 3 | 1 | 0 | 0 | 0 | 0 | 5 | 0 | 0 | 0 | 8 | 0 | 1 | 0 | 0 | 0 | 0 | 3 | 0 | 0 | 0 | 0 | 1 | 3 | 2 | 0 | 4 | 2 | 0 | 4 | 0 | **300** | 94 | 6 |
| | **SC212** | 63 | 3 | 10 | 0 | 3 | 7 | 0 | 7 | 0 | 0 | 5 | 0 | 100 | 7 | 0 | 12 | 0 | 2 | 0 | 0 | 7 | 8 | 3 | 6 | 10 | 0 | 0 | 3 | 4 | 0 | 1 | 1 | 0 | 0 | 0 | 0 | 5 | 0 | 0 | 0 | 13 | 2 | 0 | 2 | 1 | 0 | 0 | 0 | 0 | 0 | 0 | 0 | 0 | 1 | 5 | 0 | 1 | 2 | 2 | 4 | 0 | **300** | 92 | 8 |
| | **SC213** | 58 | 5 | 8 | 0 | 5 | 11 | 2 | 10 | 0 | 0 | 6 | 0 | 75 | 2 | 0 | 18 | 1 | 1 | 0 | 0 | 16 | 5 | 1 | 17 | 6 | 0 | 0 | 5 | 8 | 4 | 12 | 7 | 0 | 0 | 3 | 0 | 1 | 1 | 1 | 1 | 1 | 0 | 0 | 0 | 0 | 0 | 0 | 0 | 0 | 0 | 0 | 0 | 0 | 3 | 2 | 1 | 0 | 0 | 2 | 1 | 0 | **300** | 98 | 2 |
| | **SC214** | 56 | 5 | 6 | 1 | 0 | 10 | 2 | 13 | 0 | 1 | 1 | 2 | 88 | 4 | 0 | 14 | 4 | 0 | 0 | 0 | 28 | 9 | 7 | 12 | 4 | 0 | 0 | 0 | 9 | 0 | 4 | 9 | 0 | 0 | 1 | 0 | 0 | 0 | 0 | 0 | 2 | 1 | 0 | 0 | 0 | 0 | 0 | 0 | 1 | 0 | 0 | 0 | 0 | 3 | 0 | 0 | 0 | 0 | 3 | 0 | 0 | **300** | 99 | 1 |
| | **SC215** | 42 | 3 | 8 | 0 | 3 | 12 | 0 | 3 | 6 | 0 | 4 | 0 | 63 | 6 | 0 | 9 | 0 | 0 | 0 | 0 | 40 | 9 | 17 | 20 | 10 | 0 | 0 | 9 | 6 | 1 | 4 | 10 | 0 | 0 | 1 | 0 | 1 | 0 | 1 | 0 | 1 | 0 | 0 | 0 | 0 | 0 | 0 | 0 | 3 | 0 | 0 | 0 | 0 | 0 | 1 | 0 | 7 | 0 | 0 | 0 | 0 | **300** | 98 | 2 |
| | **SC216** | 43 | 1 | 9 | 0 | 3 | 15 | 2 | 3 | 0 | 0 | 4 | 0 | 89 | 3 | 0 | 23 | 0 | 2 | 0 | 0 | 23 | 25 | 7 | 6 | 5 | 0 | 0 | 0 | 5 | 0 | 9 | 0 | 0 | 0 | 0 | 0 | 5 | 0 | 0 | 1 | 2 | 0 | 0 | 0 | 0 | 0 | 0 | 0 | 0 | 0 | 0 | 0 | 0 | 0 | 0 | 4 | 1 | 4 | 1 | 5 | 0 | **300** | 97 | 3 |
| | **SC217** | 66 | 3 | 8 | 0 | 6 | 4 | 0 | 5 | 0 | 0 | 1 | 0 | 102 | 7 | 0 | 11 | 0 | 4 | 0 | 0 | 14 | 7 | 2 | 12 | 4 | 0 | 0 | 0 | 8 | 2 | 5 | 7 | 5 | 1 | 1 | 0 | 2 | 0 | 0 | 2 | 5 | 0 | 0 | 0 | 0 | 0 | 1 | 2 | 0 | 0 | 0 | 0 | 0 | 1 | 1 | 0 | 1 | 0 | 0 | 0 | 0 | **300** | 96 | 4 |
| | **SC218** | 63 | 3 | 8 | 0 | 3 | 8 | 0 | 13 | 0 | 0 | 3 | 0 | 98 | 3 | 0 | 13 | 1 | 0 | 0 | 0 | 10 | 11 | 2 | 7 | 7 | 0 | 0 | 4 | 6 | 1 | 1 | 7 | 0 | 0 | 0 | 0 | 7 | 0 | 0 | 0 | 3 | 1 | 0 | 0 | 2 | 1 | 0 | 0 | 3 | 0 | 0 | 0 | 0 | 1 | 3 | 0 | 2 | 2 | 3 | 0 | 0 | **300** | 94 | 6 |
| San Vicente | **SC229** | 2 | 5 | 7 | 1 | 3 | 1 | 0 | 0 | 0 | 0 | 1 | 0 | 46 | 11 | 1 | 15 | 0 | 1 | 0 | 3 | 58 | 23 | 16 | 17 | 7 | 17 | 0 | 0 | 4 | 4 | 8 | 7 | 19 | 0 | 0 | 0 | 5 | 1 | 2 | 0 | 1 | 0 | 0 | 0 | 0 | 1 | 1 | 2 | 0 | 0 | 0 | 0 | 0 | 1 | 2 | 0 | 0 | 1 | 0 | 6 | 0 | **300** | 96 | 4 |
| | **SC231** | 36 | 3 | 3 | 0 | 2 | 33 | 0 | 5 | 0 | 0 | 13 | 0 | 54 | 2 | 1 | 58 | 1 | 2 | 0 | 0 | 15 | 5 | 2 | 22 | 2 | 0 | 0 | 3 | 3 | 2 | 3 | 1 | 5 | 0 | 1 | 0 | 6 | 0 | 2 | 0 | 0 | 8 | 0 | 0 | 0 | 0 | 0 | 1 | 0 | 0 | 0 | 0 | 0 | 0 | 2 | 0 | 0 | 0 | 0 | 0 | 4 | **300** | 94 | 6 |
| | **SC234** | 35 | 5 | 4 | 0 | 4 | 25 | 0 | 5 | 0 | 1 | 15 | 0 | 80 | 2 | 5 | 42 | 1 | 0 | 0 | 0 | 23 | 4 | 3 | 13 | 2 | 0 | 0 | 5 | 2 | 3 | 2 | 0 | 3 | 0 | 1 | 0 | 0 | 0 | 0 | 0 | 1 | 0 | 0 | 0 | 3 | 2 | 1 | 3 | 1 | 0 | 0 | 0 | 0 | 0 | 2 | 0 | 1 | 0 | 0 | 1 | 0 | **300** | 96 | 4 |
| | **SC235** | 34 | 5 | 11 | 0 | 4 | 20 | 2 | 1 | 0 | 0 | 10 | 0 | 65 | 3 | 3 | 24 | 0 | 1 | 0 | 0 | 28 | 3 | 7 | 22 | 5 | 0 | 0 | 4 | 3 | 0 | 3 | 3 | 3 | 0 | 6 | 0 | 4 | 0 | 0 | 0 | 3 | 2 | 0 | 0 | 5 | 0 | 0 | 9 | 2 | 1 | 0 | 0 | 0 | 1 | 1 | 0 | 0 | 0 | 0 | 2 | 0 | **300** | 91 | 9 |
| | **SC236** | 23 | 1 | 6 | 0 | 3 | 30 | 0 | 2 | 0 | 0 | 5 | 0 | 61 | 1 | 0 | 34 | 1 | 1 | 0 | 0 | 39 | 5 | 5 | 26 | 9 | 0 | 0 | 12 | 6 | 0 | 5 | 4 | 2 | 0 | 2 | 0 | 3 | 0 | 0 | 0 | 0 | 2 | 1 | 0 | 1 | 1 | 0 | 6 | 0 | 0 | 0 | 0 | 0 | 1 | 1 | 0 | 1 | 0 | 0 | 0 | 0 | **300** | 95 | 5 |
| | **SC237** | 30 | 3 | 10 | 1 | 4 | 13 | 1 | 1 | 0 | 0 | 2 | 0 | 62 | 1 | 0 | 31 | 0 | 2 | 1 | 0 | 24 | 6 | 9 | 38 | 10 | 0 | 0 | 6 | 4 | 2 | 4 | 6 | 5 | 0 | 3 | 1 | 5 | 0 | 2 | 1 | 1 | 2 | 0 | 0 | 0 | 0 | 0 | 4 | 0 | 0 | 0 | 0 | 0 | 0 | 1 | 0 | 1 | 0 | 1 | 2 | 0 | **300** | 95 | 5 |
| El Rosaro river | **SC251** | 66 | 1 | 1 | 0 | 6 | 9 | 0 | 9 | 0 | 0 | 16 | 0 | 101 | 3 | 0 | 14 | 0 | 1 | 0 | 0 | 24 | 2 | 2 | 13 | 2 | 1 | 0 | 2 | 5 | 5 | 2 | 1 | 0 | 0 | 0 | 0 | 1 | 0 | 1 | 0 | 7 | 1 | 0 | 0 | 1 | 0 | 0 | 2 | 0 | 0 | 0 | 0 | 0 | 0 | 0 | 0 | 0 | 1 | 0 | 0 | 0 | **300** | 96 | 4 |
| | **SC260** | 51 | 2 | 3 | 0 | 6 | 11 | 1 | 9 | 0 | 1 | 10 | 0 | 116 | 3 | 0 | 19 | 1 | 3 | 1 | 0 | 15 | 4 | 2 | 7 | 4 | 0 | 0 | 2 | 6 | 3 | 3 | 1 | 1 | 0 | 0 | 0 | 2 | 0 | 0 | 0 | 7 | 4 | 0 | 0 | 1 | 0 | 0 | 1 | 0 | 0 | 0 | 0 | 0 | 0 | 0 | 0 | 0 | 0 | 0 | 0 | 0 | **300** | 95 | 5 |
| | **SC261** | 55 | 1 | 1 | 1 | 1 | 17 | 1 | 8 | 0 | 0 | 8 | 0 | 86 | 4 | 2 | 16 | 0 | 1 | 0 | 0 | 26 | 4 | 5 | 15 | 6 | 1 | 0 | 5 | 6 | 4 | 2 | 2 | 1 | 0 | 1 | 0 | 3 | 0 | 0 | 0 | 7 | 4 | 0 | 0 | 3 | 0 | 0 | 3 | 0 | 0 | 0 | 0 | 0 | 0 | 0 | 0 | 0 | 0 | 0 | 0 | 0 | **300** | 93 | 7 |
| | **SC262** | 31 | 4 | 4 | 2 | 6 | 5 | 0 | 3 | 0 | 0 | 3 | 1 | 120 | 4 | 0 | 14 | 0 | 4 | 1 | 0 | 32 | 3 | 2 | 17 | 16 | 0 | 0 | 1 | 7 | 5 | 2 | 1 | 1 | 0 | 0 | 0 | 0 | 0 | 0 | 0 | 4 | 2 | 0 | 0 | 0 | 0 | 2 | 0 | 0 | 0 | 0 | 0 | 0 | 2 | 0 | 0 | 0 | 0 | 0 | 1 | 0 | **300** | 97 | 3 |

Table

Click here to access/download;Table;Table_2.xlsx

| River | Sample | Electro-magnetic fraction | HM | tHMC* | HCI | ZTR | Titanite | Apatite | Hornblende | Tremolite | Actinolite | Other amphiboles | Augite | Diopside /hedembergite | Other clinopyroxenes | Enstatite | Hypersthene | Epidote | Garnet | Staurolite | Andalusite | Kyanite | Sillimanite |
|---|---|---|---|---|---|---|---|---|---|---|---|---|---|---|---|---|---|---|---|---|---|---|---|
| San Fernando River | SC209 | >1,5 | | | | 17 | 17 | 0 | 0 | 0 | 0 | 0 | 0 | 0 | 4 | 0 | 0 | 52 | 2 | 0 | 2 | 6 | 2 |
| | | 1.5 | | | | 31 | 41 | 0 | 2 | 0 | 0 | 0 | 2 | 2 | 2 | 0 | 0 | 19 | 2 | 0 | 0 | 0 | 0 |
| | | 1 | 2 | 1 | 33 | 4 | 0 | 0 | 55 | 0 | 0 | 0 | 23 | 1 | 0 | 0 | 0 | 15 | 1 | 0 | 0 | 0 | 0 |
| | | 0.5 | | | | 7 | 0 | 0 | 67 | 1 | 2 | 0 | 4 | 0 | 0 | 0 | 2 | 15 | 2 | 0 | 0 | 0 | 0 |
| | | 0.2 | | | | 14 | 0 | 0 | 63 | 0 | 0 | 0 | 3 | 0 | 0 | 0 | 0 | 20 | 0 | 0 | 0 | 0 | 0 |
| | SC210 | >1,5 | | | | 26 | 19 | 1 | 0 | 1 | 0 | 0 | 0 | 5 | 0 | 5 | 0 | 42 | 0 | 0 | 0 | 0 | 0 |
| | | 1.5 | | | | 36 | 41 | 0 | 0 | 0 | 0 | 0 | 0 | 2 | 0 | 0 | 0 | 20 | 0 | 0 | 0 | 0 | 2 |
| | | 1 | 7 | 5 | 33 | 21 | 6 | 0 | 6 | 0 | 0 | 0 | 15 | 2 | 0 | 0 | 0 | 46 | 2 | 2 | 0 | 0 | 0 |
| | | 0.5 | | | | 8 | 0 | 0 | 51 | 0 | 3 | 0 | 6 | 0 | 0 | 0 | 19 | 10 | 3 | 0 | 0 | 0 | 0 |
| | | 0.2 | | | | 0 | 0 | 0 | 32 | 0 | 0 | 0 | 0 | 0 | 0 | 0 | 25 | 43 | 0 | 0 | 0 | 0 | 0 |
| | SC211 | >1,5 | | | | 18 | 28 | 5 | 0 | 1 | 0 | 0 | 0 | 3 | 0 | 1 | 0 | 35 | 1 | 0 | 0 | 0 | 8 |
| | | 1.5 | | | | 21 | 60 | 0 | 0 | 0 | 0 | 0 | 2 | 0 | 0 | 0 | 0 | 17 | 0 | 0 | 0 | 0 | 0 |
| | | 1 | 6 | 5 | 26 | 7 | 9 | 0 | 26 | 2 | 0 | 2 | 19 | 9 | 0 | 0 | 2 | 21 | 2 | 0 | 0 | 0 | 0 |
| | | 0.5 | | | | 0 | 1 | 0 | 73 | 1 | 1 | 0 | 3 | 0 | 0 | 0 | 7 | 11 | 0 | 1 | 0 | 0 | 0 |
| | | 0.2 | | | | 0 | 0 | 0 | 56 | 0 | 0 | 0 | 0 | 0 | 0 | 0 | 15 | 26 | 0 | 4 | 0 | 0 | 0 |
| | SC212 | >1,5 | | | | 23 | 22 | 3 | 0 | 0 | 0 | 0 | 0 | 4 | 0 | 3 | 1 | 41 | 1 | 0 | 0 | 1 | 3 |
| | | 1.5 | | | | 62 | 26 | 0 | 0 | 0 | 0 | 0 | 0 | 1 | 0 | 0 | 1 | 6 | 1 | 1 | 0 | 0 | 0 |
| | | 1 | 4 | 3 | 43 | 5 | 0 | 0 | 12 | 0 | 0 | 0 | 29 | 2 | 0 | 0 | 5 | 43 | 0 | 5 | 0 | 0 | 0 |
| | | 0.5 | | | | 0 | 0 | 0 | 76 | 0 | 1 | 0 | 0 | 0 | 3 | 0 | 10 | 9 | 0 | 0 | 0 | 0 | 0 |
| | | 0.2 | | | | 0 | 0 | 0 | 38 | 0 | 0 | 0 | 12 | 0 | 0 | 0 | 18 | 29 | 0 | 3 | 0 | 0 | 0 |
| | SC215 | >1,5 | | | | 4 | 45 | 2 | 0 | 0 | 0 | 0 | 0 | 0 | 0 | 0 | 0 | 26 | 6 | 4 | 6 | 8 | 0 |
| | | 1.5 | | | | 2 | 83 | 0 | 0 | 0 | 0 | 0 | 0 | 0 | 2 | 0 | 0 | 6 | 2 | 4 | 0 | 0 | 0 |
| | | 1 | 2 | 1 | 28 | 3 | 0 | 0 | 40 | 0 | 13 | 0 | 10 | 0 | 7 | 3 | 0 | 23 | 0 | 0 | 0 | 0 | 0 |
| | | 0.5 | | | | 0 | 0 | 0 | 88 | 0 | 2 | 0 | 2 | 5 | 2 | 0 | 0 | 2 | 0 | 0 | 0 | 0 | 0 |
| | | 0.2 | | | | 0 | 0 | 0 | 100 | 0 | 0 | 0 | 0 | 0 | 0 | 0 | 0 | 0 | 0 | 0 | 0 | 0 | 0 |
| | SC217 | >1,5 | | | | 41 | 19 | 0 | 0 | 0 | 0 | 0 | 0 | 0 | 8 | 0 | 0 | 24 | 3 | 3 | 0 | 0 | 3 |
| | | 1.5 | | | | 23 | 65 | 0 | 0 | 0 | 0 | 0 | 0 | 0 | 2 | 2 | 0 | 8 | 0 | 0 | 0 | 0 | 0 |
| | | 1 | 13 | 13 | 40 | 17 | 2 | 0 | 11 | 0 | 2 | 0 | 2 | 0 | 11 | 0 | 9 | 36 | 6 | 4 | 0 | 0 | 0 |
| | | 0.5 | | | | 0 | 0 | 0 | 67 | 0 | 0 | 0 | 1 | 0 | 0 | 0 | 9 | 16 | 3 | 3 | 0 | 0 | 0 |
| | | 0.2 | | | | 12 | 0 | 0 | 62 | 0 | 0 | 0 | 0 | 0 | 12 | 0 | 0 | 12 | 0 | 4 | 0 | 0 | 0 |
| | SC218 | >1,5 | | | | 22 | 9 | 0 | 0 | 0 | 0 | 0 | 0 | 0 | 0 | 0 | 0 | 58 | 2 | 0 | 0 | 2 | 8 |
| | | 1.5 | | | | 25 | 60 | 0 | 0 | 0 | 0 | 0 | 2 | 0 | 0 | 0 | 0 | 11 | 0 | 0 | 0 | 0 | 4 |
| | | 1 | 8 | 5 | 31 | 5 | 0 | 0 | 24 | 0 | 2 | 2 | 10 | 2 | 5 | 0 | 0 | 44 | 5 | 0 | 0 | 0 | 0 |
| | | 0.5 | | | | 0 | 0 | 0 | 64 | 0 | 2 | 0 | 0 | 2 | 0 | 0 | 13 | 11 | 4 | 5 | 0 | 0 | 0 |
| | | 0.2 | | | | 0 | 0 | 0 | 35 | 0 | 3 | 0 | 0 | 0 | 0 | 0 | 42 | 16 | 0 | 3 | 0 | 0 | 0 |
| San Vicente River | SC229 | >1,5 | | | | 20 | 40 | 0 | 0 | 0 | 0 | 0 | 7 | 0 | 0 | 0 | 3 | 27 | 3 | 0 | 0 | 0 | 0 |
| | | 1.5 | | | | 22 | 56 | 4 | 0 | 0 | 0 | 0 | 4 | 0 | 0 | 0 | 4 | 11 | 0 | 0 | 0 | 0 | 0 |
| | | 1 | 1 | 1 | 32 | 0 | 0 | 0 | 86 | 0 | 0 | 0 | 0 | 0 | 0 | 0 | 0 | 14 | 0 | 0 | 0 | 0 | 0 |
| | | 0.5 | | | | 0 | 0 | 0 | 38 | 0 | 0 | 0 | 0 | 0 | 0 | 0 | 0 | 63 | 0 | 0 | 0 | 0 | 0 |
| | | 0.2 | | | | 0 | 0 | 0 | 79 | 0 | 11 | 0 | 0 | 0 | 0 | 0 | 0 | 11 | 0 | 0 | 0 | 0 | 0 |
| | SC231 | >1,5 | | | | 19 | 44 | 0 | 0 | 0 | 0 | 0 | 0 | 0 | 0 | 0 | 0 | 30 | 0 | 0 | 0 | 0 | 7 |
| | | 1.5 | | | | 12 | 78 | 0 | 0 | 0 | 0 | 0 | 0 | 0 | 0 | 0 | 0 | 8 | 0 | 0 | 0 | 0 | 2 |
| | | 1 | 1 | 1 | 35 | 8 | 8 | 0 | 58 | 0 | 12 | 0 | 0 | 0 | 0 | 0 | 0 | 15 | 0 | 0 | 0 | 0 | 0 |
| | | 0.5 | | | | 0 | 0 | 0 | 81 | 0 | 0 | 5 | 0 | 0 | 0 | 0 | 0 | 14 | 0 | 0 | 0 | 0 | 0 |
| | | 0.2 | | | | 0 | 0 | 0 | 91 | 0 | 0 | 3 | 0 | 0 | 0 | 0 | 0 | 6 | 0 | 0 | 0 | 0 | 0 |
| | SC235 | >1,5 | | | | 14 | 49 | 2 | 0 | 0 | 0 | 0 | 0 | 0 | 0 | 3 | 0 | 22 | 3 | 2 | 0 | 0 | 5 |
| | | 1.5 | | | | 8 | 84 | 0 | 0 | 0 | 0 | 0 | 2 | 0 | 0 | 0 | 0 | 4 | 0 | 2 | 0 | 0 | 0 |
| | | 1 | 7 | 5 | 41 | 7 | 7 | 0 | 60 | 0 | 0 | 0 | 0 | 0 | 0 | 0 | 0 | 27 | 0 | 0 | 0 | 0 | 0 |
| | | 0.5 | | | | 8 | 0 | 0 | 50 | 0 | 0 | 0 | 0 | 0 | 0 | 0 | 0 | 42 | 0 | 0 | 0 | 0 | 0 |
| | | 0.2 | | | | 0 | 0 | 0 | 86 | 0 | 0 | 0 | 0 | 0 | 0 | 0 | 0 | 14 | 0 | 0 | 0 | 0 | 0 |
| El Rosario River | SC251 | >1,5 | | | | 44 | 44 | 6 | 0 | 0 | 0 | 0 | 0 | 0 | 0 | 0 | 0 | 6 | 0 | 0 | 0 | 0 | 0 |
| | | 1.5 | | | | 4 | 93 | 0 | 0 | 0 | 0 | 0 | 0 | 0 | 0 | 0 | 0 | 0 | 0 | 4 | 0 | 0 | 0 |
| | | 1 | 8 | 7 | 31 | 10 | 5 | 0 | 52 | 0 | 0 | 0 | 10 | 0 | 0 | 0 | 0 | 24 | 0 | 0 | 0 | 0 | 0 |
| | | 0.5 | | | | 0 | 0 | 0 | 82 | 0 | 0 | 0 | 0 | 0 | 0 | 0 | 13 | 4 | 0 | 0 | 0 | 0 | 0 |
| | | 0.2 | | | | 0 | 0 | 0 | 95 | 0 | 0 | 0 | 0 | 0 | 2 | 0 | 2 | 0 | 0 | 0 | 0 | 0 | 0 |
| | SC260 | >1,5 | | | | 10 | 88 | 0 | 0 | 0 | 0 | 0 | 0 | 0 | 0 | 0 | 0 | 0 | 0 | 1 | 0 | 0 | 0 |
| | | 1.5 | | | | 12 | 88 | 0 | 0 | 0 | 0 | 0 | 0 | 0 | 0 | 0 | 0 | 0 | 0 | 0 | 0 | 0 | 0 |
| | | 1 | 34 | 28 | 32 | 0 | 4 | 0 | 19 | 0 | 0 | 0 | 0 | 0 | 0 | 0 | 0 | 77 | 0 | 0 | 0 | 0 | 0 |
| | | 0.5 | | | | 0 | 0 | 0 | 84 | 0 | 0 | 0 | 0 | 0 | 0 | 0 | 13 | 3 | 0 | 0 | 0 | 0 | 0 |
| | | 0.2 | | | | 0 | 3 | 0 | 68 | 0 | 0 | 0 | 0 | 0 | 0 | 0 | 29 | 0 | 0 | 0 | 0 | 0 | 0 |
| | SC261 | >1,5 | | | | 8 | 71 | 0 | 0 | 0 | 0 | 0 | 0 | 0 | 5 | 0 | 0 | 8 | 3 | 0 | 0 | 5 | 0 |
| | | 1.5 | | | | 16 | 84 | 0 | 0 | 0 | 0 | 0 | 0 | 0 | 0 | 0 | 0 | 0 | 0 | 0 | 0 | 0 | 0 |
| | | 1 | 9 | 7 | 35 | 0 | 7 | 0 | 54 | 0 | 0 | 0 | 4 | 0 | 18 | 0 | 4 | 11 | 4 | 0 | 0 | 0 | 0 |
| | | 0.5 | | | | 2 | 0 | 0 | 81 | 0 | 2 | 2 | 0 | 0 | 0 | 0 | 13 | 2 | 0 | 0 | 0 | 0 | 0 |
| | | 0.2 | | | | 0 | 6 | 0 | 41 | 0 | 0 | 0 | 0 | 0 | 0 | 0 | 41 | 12 | 0 | 0 | 0 | 0 | 0 |

*tHMC=not magnetic fraction to the Frantz magnetic separator

 

| Sample | River | Geographic coordinates |
|---|---|---|
| SC251 | El Rosario | 30°03'55.841"N 115°42'2765"W |
| SC260 | | 30°02'14.578"N 115°45'19.688"W |
| SC261 | | 30°06'52.675"N 115°38'53.932"W |
| SC262 | | 30°09'5.718"N 115°35'20.111"W |
| SC229 | San Vicente | 29°58'10.536 N 115°22'28.448"W |
| SC231 | | 29°44'26.634N 115°39'18,261"W |
| SC234 | | 29°50'54.596"N 115°35'33,144"W |
| SC235 | | 29°53'21.508"N 115°32'41,216"W |
| SC236 | | 29°55'49,69"N 115°28'11.568"W |
| SC237 | | 29°57'1.604"N 115°22'28.448"W |
| SC209 | San Fernando | 29°48'25.395"N 115°29'31.31"W |
| SC210 | | 29°57'59.343"N 115°13'9.458"W |
| SC211 | | 29°57'28.772"N 115°07'36.248"W |
| SC212 | | 29°44'26.634"N 115°38'45.818"W |
| SC213 | | 30°01'28.085N 114°49'51.094"W |
| SC214 | | 29°59'23.869"N 114°52'49.509"W |
| SC215 | | 30°03'3.905"N 114°49'4.082"W |
| SC216 | | 29°58'38.071N 114°54'24.007"W |
| SC217 | | 29°54'51.582"N 115°19'50.814"W |
| SC218 | | 29°51'50.325"N 115°26'3.829"W |

| River | Sample | Qm | F | Lt | | Qt | F | L | | Qm | K | P | | Qp | Lvm | Lsm | | Lm | Lv | Ls | | Ls | Lm1 | Lm2 | | Rg | Rv | Rm | |
|---|---|---|---|---|---|---|---|---|---|---|---|---|---|---|---|---|---|---|---|---|---|---|---|---|---|---|---|---|---|
| San Fernando | **SC209** | 21 | 54 | 25 | **100** | 25 | 54 | 21 | **100** | 28 | 2 | 70 | **100** | 17 | 50 | 33 | **100** | 3 | 61 | 36 | **100** | 85 | 0 | 15 | **100** | 23 | 70 | 7 | **100** |
| | **SC210** | 20 | 49 | 31 | **100** | 23 | 49 | 28 | **100** | 29 | 8 | 63 | **100** | 11 | 76 | 13 | **100** | 7 | 85 | 8 | **100** | 0 | 0 | 100 | **100** | 20 | 70 | 10 | **100** |
| | **SC211** | 18 | 50 | 32 | **100** | 22 | 50 | 28 | **100** | 27 | 6 | 67 | **100** | 12 | 64 | 24 | **100** | 8 | 72 | 20 | **100** | 40 | 0 | 60 | **100** | 23 | 64 | 13 | **100** |
| | **SC212** | 27 | 49 | 24 | **100** | 32 | 49 | 19 | **100** | 36 | 6 | 58 | **100** | 20 | 57 | 23 | **100** | 8 | 71 | 21 | **100** | 33 | 0 | 67 | **100** | 33 | 58 | 9 | **100** |
| | **SC213** | 26 | 38 | 36 | **100** | 30 | 38 | 32 | **100** | 40 | 9 | 51 | **100** | 12 | 48 | 40 | **100** | 13 | 54 | 33 | **100** | 61 | 0 | 39 | **100** | 33 | 50 | 17 | **100** |
| | **SC214** | 23 | 42 | 35 | **100** | 26 | 42 | 32 | **100** | 35 | 9 | 56 | **100** | 10 | 59 | 31 | **100** | 9 | 66 | 25 | **100** | 59 | 0 | 41 | **100** | 25 | 65 | 10 | **100** |
| | **SC215** | 20 | 29 | 51 | **100** | 24 | 29 | 47 | **100** | 40 | 5 | 55 | **100** | 7 | 72 | 21 | **100** | 5 | 78 | 17 | **100** | 68 | 0 | 32 | **100** | 18 | 75 | 7 | **100** |
| | **SC216** | 22 | 43 | 35 | **100** | 26 | 43 | 31 | **100** | 34 | 4 | 62 | **100** | 10 | 66 | 24 | **100** | 6 | 73 | 21 | **100** | 64 | 0 | 36 | **100** | 35 | 57 | 8 | **100** |
| | **SC217** | 27 | 44 | 29 | **100** | 31 | 44 | 25 | **100** | 38 | 3 | 59 | **100** | 13 | 49 | 38 | **100** | 15 | 55 | 30 | **100** | 63 | 0 | 37 | **100** | 20 | 57 | 23 | **100** |
| | **SC218** | 26 | 47 | 27 | **100** | 30 | 47 | 23 | **100** | 38 | 8 | 54 | **100** | 14 | 56 | 30 | **100** | 11 | 65 | 24 | **100** | 53 | 0 | 47 | **100** | 34 | 54 | 12 | **100** |
| | | | | | | | | | | | | | | | | | | **85** | **680** | **235** | | **526** | **0** | **474** | | | | | |
| San Vicente | **SC229** | 3 | 27 | 70 | **100** | 7 | 27 | 66 | **100** | 9 | 1 | 90 | **100** | 6 | 71 | 23 | **100** | 4 | 75 | 21 | **100** | 64 | 0 | 36 | **100** | 12 | 82 | 6 | **100** |
| | **SC231** | 26 | 48 | 26 | **100** | 28 | 48 | 24 | **100** | 35 | 9 | 56 | **100** | 8 | 68 | 24 | **100** | 8 | 74 | 18 | **100** | 50 | 0 | 50 | **100** | 65 | 30 | 5 | **100** |
| | **SC234** | 22 | 53 | 25 | **100** | 25 | 53 | 22 | **100** | 30 | 10 | 60 | **100** | 12 | 69 | 19 | **100** | 8 | 78 | 14 | **100** | 75 | 0 | 25 | **100** | 56 | 34 | 10 | **100** |
| | **SC235** | 22 | 39 | 39 | **100** | 28 | 39 | 33 | **100** | 36 | 7 | 57 | **100** | 15 | 65 | 20 | **100** | 3 | 77 | 20 | **100** | 65 | 0 | 35 | **100** | 41 | 52 | 7 | **100** |
| | **SC236** | 20 | 38 | 42 | **100** | 23 | 38 | 39 | **100** | 35 | 4 | 61 | **100** | 6 | 75 | 19 | **100** | 6 | 79 | 15 | **100** | 71 | 0 | 29 | **100** | 43 | 51 | 6 | **100** |
| | **SC237** | 18 | 35 | 47 | **100** | 22 | 35 | 43 | **100** | 34 | 2 | 64 | **100** | 10 | 70 | 20 | **100** | 5 | 78 | 17 | **100** | 81 | 0 | 19 | **100** | 32 | 61 | 7 | **100** |
| | | | | | | | | | | | | | | | | | | **34** | **461** | **105** | | **406** | **0** | **194** | | | | | |
| El Rosario | **SC251** | 28 | 50 | 22 | **100** | 29 | 50 | 21 | **100** | 36 | 11 | 53 | **100** | 3 | 74 | 23 | **100** | 17 | 76 | 7 | **100** | 23 | 0 | 77 | **100** | 39 | 46 | 15 | **100** |
| | **SC260** | 25 | 56 | 19 | **100** | 26 | 56 | 18 | **100** | 30 | 9 | 61 | **100** | 9 | 65 | 26 | **100** | 19 | 71 | 10 | **100** | 36 | 0 | 64 | **100** | 45 | 38 | 17 | **100** |
| | **SC261** | 27 | 44 | 29 | **100** | 28 | 44 | 28 | **100** | 38 | 8 | 54 | **100** | 3 | 77 | 20 | **100** | 13 | 79 | 8 | **100** | 33 | 0 | 67 | **100** | 36 | 54 | 10 | **100** |
| | **SC262** | 15 | 51 | 34 | **100** | 18 | 51 | 31 | **100** | 23 | 4 | 73 | **100** | 8 | 73 | 19 | **100** | 13 | 80 | 7 | **100** | 25 | 0 | 75 | **100** | 20 | 64 | 16 | **100** |
| | | | | | | | | | | | | | | | | | | **62** | **306** | **32** | | **117** | **0** | **283** | | | | | |
| | | **436** | **886** | **678** | | **503** | **886** | **611** | | **651** | **125** | **1224** | | **206** | **1304** | **490** | | **181** | **1447** | **372** | | **1049** | **0** | **951** | | **653** | **1132** | **215** | |

| River | Sample | Lvmi | Lvl | Lvv | Lvfgr | Lvfser | Lvalt/und | Tot |
|---|---|---|---|---|---|---|---|---|
| San Fernando | **SC209** | 50 | 3 | 0 | 18 | 19 | 10 | **100** |
| | **SC210** | 49 | 12 | 0 | 15 | 18 | 6 | **100** |
| | **SC211** | 47 | 10 | 0 | 22 | 13 | 8 | **100** |
| | **SC212** | 55 | 6 | 0 | 17 | 19 | 3 | **100** |
| | **SC213** | 51 | 4 | 1 | 23 | 9 | 12 | **100** |
| | **SC214** | 74 | 7 | 0 | 11 | 4 | 4 | **100** |
| | **SC215** | 62 | 1 | 6 | 10 | 10 | 11 | **100** |
| | **SC216** | 60 | 4 | 2 | 13 | 13 | 8 | **100** |
| | **SC217** | 45 | 4 | 0 | 22 | 19 | 10 | **100** |
| | **SC218** | 50 | 1 | 0 | 18 | 17 | 14 | **100** |
| | | **543** | **52** | **9** | **169** | **141** | **86** | |
| San Vicente | **SC237** | 50 | 11 | 5 | 17 | 7 | 10 | **100** |
| | **SC229** | 69 | 4 | 0 | 20 | 5 | 2 | **100** |
| | **SC231** | 62 | 3 | 2 | 17 | 5 | 11 | **100** |
| | **SC234** | 71 | 6 | 1 | 8 | 5 | 9 | **100** |
| | **SC235** | 59 | 5 | 1 | 17 | 5 | 13 | **100** |
| | **SC236** | 41 | 19 | 2 | 24 | 14 | 0 | **100** |
| | | **352** | **48** | **11** | **103** | **41** | **45** | |
| El Rosaro | **SC251** | 49 | 6 | 2 | 15 | 23 | 5 | **100** |
| | **SC260** | 60 | 10 | 6 | 6 | 18 | 0 | **100** |
| | **SC261** | 54 | 5 | 4 | 7 | 29 | 1 | **100** |
| | **SC262** | 49 | 1 | 2 | 9 | 38 | 1 | **100** |
| | | **212** | **22** | **14** | **37** | **108** | **7** | |
| | | **1671** | **192** | **59** | **449** | **439** | **190** | |